CARBON DIOXIDE CAPTURE BY COPPER OXIDE NANOPARTICLES DECORATED SUPPORTS

A THESIS SUBMITTED TO
THE GRADUATE SCHOOL OF NATURAL AND APPLIED SCIENCES
OF
MIDDLE EAST TECHNICAL UNIVERSITY

BY

CANSU BÖRÜBAN

IN PARTIAL FULFILLMENT OF THE REQUIREMENTS
FOR
THE DEGREE OF MASTER OF SCIENCE
IN
CHEMISTRY

JANUARY 2016

Approval of the thesis:

CARBONDIOXIDE CAPTURE BY COPPER OXIDE NANOPARTICLES DECORATED SUPPORTS

submitted by **CANSU BÖRÜBAN in** partial fulfillment of the requirements for the degree of **Master of Science in Chemistry Department, Middle East Technical University** by,

Prof. Dr. Gülbin Dural Ünver _____
Dean, Graduate School of **Natural and Applied Sciences**

Prof. Dr. Cihangir Tanyeli _____
Head of Department, **Chemistry**

Assoc. Prof. Dr. Emren Nalbant Esentürk _____
Supervisor, **Chemistry Department, METU**

Examining Committee Members:

Prof. Dr. Ceyhan Kayran _____
Chemistry Dept., METU

Assoc. Prof. Dr. Emren Nalbant Esentürk _____
Chemistry Dept., METU

Prof. Dr. Nurşen Altuntaş Öztaş _____
Chemistry Dept., Hacettepe University

Prof. Dr. Ayşen Yılmaz _____
Chemistry Dept., METU

Assoc. Prof. Dr. Gülay Ertaş _____
Chemistry Dept., METU

Date: 25. 01. 2016

I hereby declare that all information in this document has been obtained and presented in accordance with academic rules and ethical conduct. I also declare that, as required by these rules and conduct, I have fully cited and referenced all material and results that are not original to this work.

Name, Last Name: Cansu BÖRÜBAN

Signature:

ABSTRACT

CARBONDIOXIDE CAPTURE BY COPPER OXIDE NANOPARTICLES DECORATED SUPPORTS

Börüban, Cansu
M. S., Department of Chemistry
Supervisor: Assoc. Prof. Dr. Emren Nalbant Esentürk
January 2016, 92 Pages

Carbon dioxide (CO_2) is the primary greenhouse gas emitted through human activities such as combustion of fossil fuels (coal, natural gas, and oil) for energy and transportation. The amount of CO_2 released to the atmosphere can be decreased by using CO_2 adsorbing materials.

Zeolites and activated carbons outshine with their high surface areas for the purpose of adsorbing gas molecules. Their highly porous, three dimensional structures makes them great host to trap gas molecules and purifying industrial gases. Modifying the surface of these dry adsorbents with metal oxide nanoparticles which preferentially capture certain gases is considered as an attractive route to enhance their selectivity as well as their gas trapping and storing efficiency.

In this study, improving the CO_2 adsorption and storing ability of activated carbon and zeolite by integrating copper oxide nanoparticles onto the surface of these supports was aimed. The synthesis of copper oxide (Copper(I) oxide (Cu_2O) and Copper(II) oxide (CuO)) nanoparticles were synthesized on the adsorbent surfaces by precipitation method. Characterization of copper oxide decorated adsorbents' morphological, chemical and gas capturing capabilities were performed by X-Ray

Diffraction Spectroscopy (XRD), Fourier Transform Infrared Spectroscopy (FTIR), X-Ray Photoelectron Spectroscopy (XPS), Transmission Electron Microscopy (TEM), Scanning Electron Microscopy (SEM), Energy-dispersive X-ray spectroscopy (EDX). Analysis of adsorbed CO_2 was done by Thermo gravimetric Analysis (TGA), and Brunauer-Emmett-Teller (BET) studies.

The developed hybrid system has provided the adsorption of CO_2 on the copper oxide nanoparticles by chemically compared to its relatively weak adsorption on zeolite and activated carbon.

Key Words: Nanoparticles, copper oxide, carbon dioxide, adsorption, surface, zeolite, activated carbon, porous structure, dry adsorbents.

ÖZ

BAKIR OKSİT NANOPARÇAÇIKLAR YERLEŞTİRİLMİŞ ADSORBANLAR TARAFINDAN KARBONDİOKSİT TUTUNUMU

Börüban, Cansu
Yüksek Lisans, Kimya Bölümü
Tez Yöneticisi: Doç. Dr. Emren Nalbant Esentürk
Ocak 2016, 92 Sayfa

Karbon dioksit (CO_2), enerji ve ulaşım için fosil yakıtların (kömür, doğal gaz ve petrol) yakılması gibi insan faaliyetleri yoluyla yayılan birincil sera gazıdır. Atmosfere salınan CO_2 miktarı, CO_2 gazını adsorbe eden malzemeler kullanılarak azaltılabilir.

Zeolit ve aktif karbon, yüksek yüzey alanı ve gözenekli yapısı sayesinde gaz moleküllerinin tutunumunda kullanılan adsorbanlardır. Yüksek gözenekli ve üç boyutlu yapısı, zeolit ve aktif karbonu gaz moleküllerinin tutunumunda ve endüstriyel gazların ayırımında iyi birer ev sahibi yapar. Bu kuru adsorbanların gaz yakalama ve depolama verimliliğini artırmak amacıyla yüzey yapısının özellikle belirli gazların tutunumunda kullanmak için metal oksit nanoparçacıkları yardımıyla değiştirilmesi ilgi çeken bir yol olarak kabul edilir.

Bu çalışmada aktif karbon ve zeolitin yüzeylerine bakır oksit nanoparçacıkları tutturularak, malzemelerin CO_2 tutma ve depolama özelliklerinin geliştirilmesi amaçlanmıştır. Yüzey üzerine bakır (I) oksit (Cu_2O) ve bakır (II) oksit (CuO) nanoparçacıkları çökeltme metoduyla sentezlenmiştir. Bakır oksit yüklenmiş adsorbanların morfolojik, kimyasal ve gaz yakalama özellikleri X-ışınları kırınım

cihazı (XRD), Fourier Dönüşümlü Infrared Spektrofotometre (FTIR), X-Işını Fotoelektron Spektroskopisi (XPS), Yüksek Çözünürlüklü Transmisyon Elektron Mikroskobu (TEM), Taramalı Elektron Mikroskobu (SEM) ve Enerji Dağılımlı X-Işını Spektroskopisi (EDX) kullanılarak karakterize edilmiştir. Tutunan CO_2 analizi Thermogravimetrik Analiz (TGA) cihazı ve Yüksek Çözünürlüklü Yüzey Alanı ve Mikro Gözenek Boyutu Analiz Cihazi (BET) çalışmalarıyla yapılmıştır.
Geliştirilen hibrit sistemde, bakır oksit nanoparçacıkları yardımıyla, zeolit ve aktif karbona kıyasla daha güçlü bir şekilde CO_2 tutunumu sağlanmıştır.

Anahtar Kelimeler: Nanoparçacık, bakır oksit, karbondioksit, adsorpsiyon, yüzey, zeolit, aktif karbon, gözenekli yapı, kuru adsorbanlar

to my precious family…

ACKNOWLEDGEMENTS

First of all, I would like to thank my advisor Assoc. Prof. Dr. Emren NALBANT ESENTÜRK for her continuous support and motivation. Her guidance helped me in all the time of research and writing of this thesis. She was always there to listen and to give advice.

I would like to express my special appreciation to Assoc. Prof. Dr. Okan ESENTÜRK for his contribution to this work, insightful comments, immeasurable patience, and accessibility. He showed me different ways to approach a research problem.

I am grateful to Assoc. Prof. Dr. Gülay ERTAŞ for her valuable help. She has always been available to answer my questions and clear any doubts that I had.

I would like to send my appreciation to Prof. Dr. Jale HACALOĞLU for access to TGA Instrument and Prof. Dr. Ayşen YILMAZ for access to XRD Instrument.

Special thank goes to my fellow lab-mates who supported me during my time here; Asude ÇETİN, N. İlkem EVCİMEN, and S. Esra ÖĞÜN for their endless friendship, continuous moral support, and standing by me in my hard times during this work and they have willingly helped me out with their abilities; Çiğdem ACAR, Serra KARAMAN, Asena AVCI, Aylin ELÇİ, and Emir AYDIN for providing me a friendly and cheerful group. I am lucky to have met them.

I would like to express my deepest appreciation to İlkay YAZGI for his invaluable friendship and generous support.

Most importantly, none of this would have been possible without the love of my family; my mother Ganime BÖRÜBAN, my father Ali İhsan BÖRÜBAN, and my sister Özge BÖRÜBAN. They have always helped me at every stage of my personal and academic life. I really appreciate their belief in me and encouraging me with their best wishes. You made me live most unique, magic, and carefree childhood that have made me who I am now.

TABLE OF CONTENTS

LIST OF FIGURES

FIGURES

LIST OF TABLES

TABLES

LIST OF ABBREVIATIONS

^{o}	degrees
^{o}C	degrees Celsius
BET	Brunauer, Emmett and Teller Theory
ca.	Circa (prediction in amount)
cm^3	cubic centimeter
EDX	Energy Dispersive X-ray Spectroscopy
et al.	et alii (and others)
eV	electron Volts
FTIR	Fourier Transform Infrared Spectroscopy
g	gram
i.e	id est (in essence)
K	Kelvin
m^2	square meters
M	molarity
mm	millimeter
mg	milligram
mL	milliliter
mmol	millimole
mM	millimolar
nm	nanometer
SEM	Scanning Electron Microscopy
TEM	Transmission Electron Microscopy
TGA	Thermogravimetric Analysis
XRD	X-Ray Diffraction
XPS	X-ray Photoelectron Spectroscopy

CHAPTER 1

INTRODUCTION

1.1. Motivation for the Study

Greenhouse effect is a natural phenomenon; however, excessive release of various harmful gases into the atmosphere by humans results in an uncontrollable increase in the average temperature of the world. Water vapor, carbon dioxide, methane and nitrous gases are some examples of the greenhouse gases causing greenhouse effect and thus global warming. Among these gases carbon dioxide (CO_2) which is mostly produced by the use of C-based fuels, making significant contribution to this effect. There are some important precautions that can be taken to reduce CO_2 emissions; (i) improvement of energy efficiency, (ii) preventing deforestation, (iii) giving priority to new energy production technologies, (iv) using non-carbon energy sources, and (v) developing carbon capture and storage technologies.

Among all these precautions, CO_2/carbon capture and storage technology is one of the most promising and well-accepted one in recent years. Solid adsorbents with highly porous structures such as zeolites and activated carbon are great candidates to implement this technology. There is an increasing attention toward using these adsorbents in CO_2 capturing as well as enhancing their adsorbing and storing capabilities. This can be achieved either by modifying their surface chemistry in a way to attract more CO_2 or by decorating them with metal oxide nanoparticles. The second approach is particularly intriguing as it embodies the unique advantages of nanoparticles such as having high surface to volume ratio. Implanting these particles onto the support surface lead to increase in the surface

area where more gas molecules can be adsorbed. In addition, the nanoparticles with chemical characteristics which provide selectivity toward specific gas molecules are suggested to result significant improvement in the adsorption properties of these supports.

The use of copper oxide nanoparticles in metal oxide-support hybrid system is a very promising approach due to their basic character that selectively attract acidic CO_2 and being cost-effective. The synthesis of copper oxide (CuO and Cu_2O) nanoparticles on zeolite surface has been successfully achieved.[1–3] However, CO_2 adsorbing capabilities of this system has not been discussed. In another report, both preparation of copper oxide film on activated carbon surface and the CO_2 adsorption properties of this hybrid system have been discussed.[4] However, to best of our knowledge, CO_2 adsorption properties of copper oxide particles in nanoscale loaded on activated carbon or zeolite supports have not been reported, yet.

This thesis study focuses on synthesis of copper oxide (CuO and Cu_2O) nanoparticles on zeolite and activated carbon surfaces as well as the investigation of their CO_2 adsorbing properties.

1.2.Global Warming and Low Carbon Economy

Generation of greenhouse gases resulting from human activities is becoming an important concern all over the world. Greenhouse gases trap some of the heat coming from the sun and make an important contribution to the greenhouse effect. Greenhouse effect is a natural process in which methane, carbon dioxide, water vapor, and other greenhouse gases absorb the beam reflecting from the surface and it causes increase in Earth's temperature.[5]

The certain greenhouse gases contributing to global warming in the atmosphere are water vapor (H_2O), methane (CH_4) nitrous oxide (N_2O), fluorinated gases (F-gases), and carbon dioxide (CO_2).[6] Water vapor is the most abundant greenhouse gas in the atmosphere. Increases in the amount of water vapor in the atmosphere causes the formation of clouds and it acts as a feedback mechanism to the climate change. CH_4 is the second prevalent greenhouse gases in the atmosphere and it is a hydrocarbon gas produced both petroleum systems and human activities.[7] N_2O is one of the most powerful greenhouse gases generated by usage of synthetic fertilizer, burning of fuels, and as a byproduct of nitric acid.[7] Fluorinated gases have no natural sources. Only human-related activities causes the formation of fluorinated gases that includes hydrofluorocarbons (HFCs), perfluorocarbons (PFCs), sulfur hexafluoride (SF_6), and nitrogen trifluoride (NF_3).[8] CO_2 is the primary greenhouse gas resulted from human activities and natural processes.

At the global scale, the percentages of the emission of greenhouse gases into the atmosphere are given in Figure 1.1. The percentage of CO_2 emission into the atmosphere is assumed that CO_2 has the greatest impact on greenhouse effect compared to other greenhouse gases.

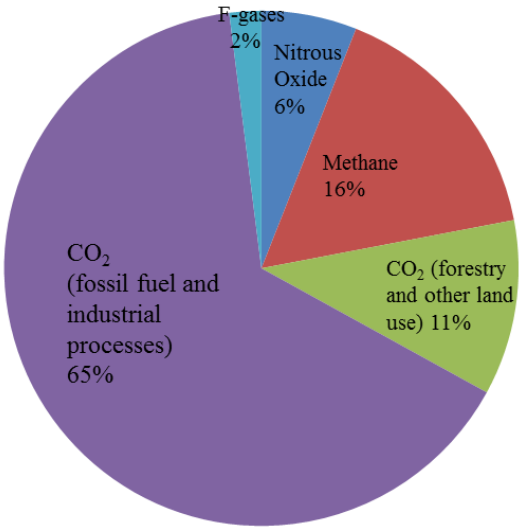

Figure 1.1. Global greenhouse gas emissions. Adapted from reference 9.

The carbon suppliers in the atmosphere, soils, oceans and rocks are related to a complex natural biochemical process called carbon cycle.[10] CO_2 is naturally present in the atmosphere as a part of carbon cycle. Natural sources, human activities, and burning of fossil fuels altering the carbon cycle by adding or consuming CO_2.[11] Respiration and volcano eruption can be given as examples of natural sources of CO_2. Human activities such as deforestation are attributed to CO_2 emission as well as natural sources. However; the major contribution to the amount of emitted CO_2 to the atmosphere comes from the combustion of fossil fuels like coal, coke, and natural gas.[12] Beside the burning of fossil fuels, the fermentation of carbohydrate materials and production of cement and lime also make the quantity of CO_2 in the atmosphere increase.[13]

Figure 1.2 shows the proportion of CO_2 emitted by the various sectors of the global economy. On the right side, indirect emissions are shown and direct emissions are shown on the left side. It is estimated from the graph that thermoelectric power plants (combustion of fossil fuels for heat and electricity production), industrial plants (steel industry), and AFOLU (agriculture, forestry,

and other land use) are the major sources of CO_2 emission into the atmosphere.[14] Furthermore; transportation, other energy, and building-related emissions make contribution to emitted CO_2.

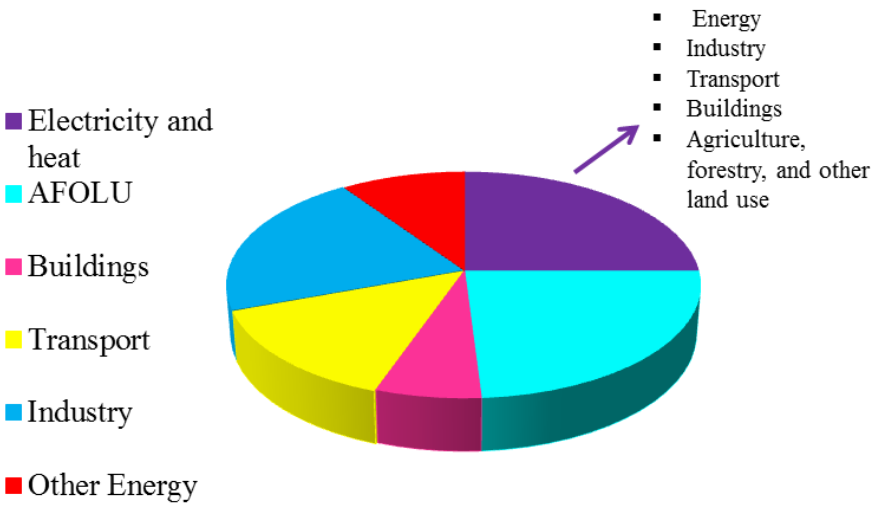

Figure 1.2. CO_2 gas emission by economic sectors Adapted from reference 15.

The CO_2 level on the atmosphere have increased by over 30% compared to pre-industrial levels.[16] Intergovernmental Panel on Climate Change (IPCC) estimates that the atmosphere will contain more than 700 ppm (v) carbon dioxide in the year 2100 and present concentration of CO_2 is approximately 400 ppm(v). [17]

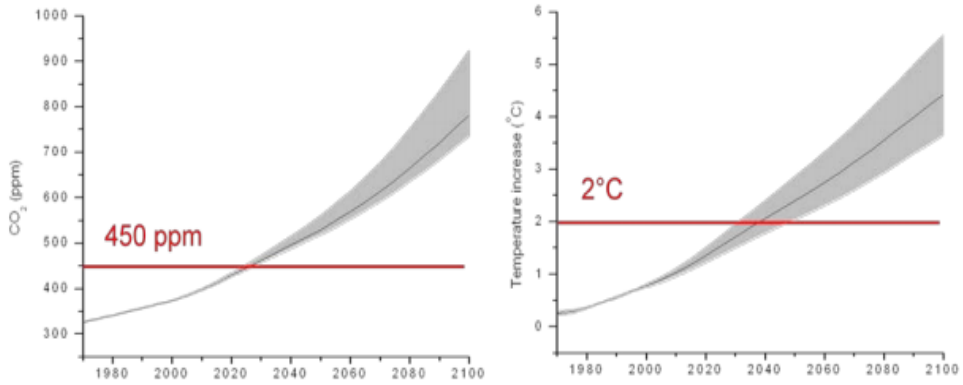

Figure 1.3. Long-run CO2 concentrations and temperature increase: Baseline, 1980-2100. Adapted from reference 15**.**

Organization for Economic Co-operation and Development (OECD) estimates that a CO_2 concentration of 450 ppm would result in a global temperature rise of 2 degrees Celsius (°C) above pre-industrial levels by 2100 (Figure 1.3). Surpassing the temperature rise above 2 °C would cause altering precipitation patterns, ice fields melting, and rising of see levels. These consequences drug the Earth into a bad situation. Life on Earth is endangered. Therefore; removal of excess CO_2 is important. Because of these global concerns, strict global regulations about CO_2 emission have been implemented. Awareness of greenhouse gas emission and contribution of these gases (especially CO_2) to the greenhouse effect has been gained via the Kyoto Protocol.[14] According to this protocol, industrialized countries that have responsibilities for the high level of greenhouse gases into the atmosphere have to limit their emitted greenhouse gases. A variety of industries have to obey these regulations. Because of that obligation, some approaches have been developed to reduce anthropogenic CO_2 emission. Use of fuels with low carbon content, nuclear energy, renewable energy sources, and capturing and storing CO_2 are the ways to lower emitted CO_2 amount.[18] However; due to the economic concerns, carbon capture and storage have gained a great interest for long term technology policies.[6]

CO_2 is generally used in beverages to carbonate soft drinks and soda waters, neutralization of alkaline waste water produced by iron-steel, dyeing, textile, and paper industry, welding as CO_2 laser, chemical industry to produce urea, methanol, soda ash etc., freezing of food products, and oil recovery from oil wells.[19–21]

1.3.CO_2 Capture and Storage Technology (CCS)

The rise in Earth's temperature is mostly result of increasing the concentration of CO_2 commonly emitted by burning of fossil fuels.[22] The majority of the worlds' energy need is provided by fossil fuel power plants involving coal, oil, and gas.[5] Carbon capture and storage is widely used technique for limiting the emitted CO_2 which is the primary greenhouse gas changing global climate from the fossil fuel power plants.[6] The summary of basic CCS concept is given in Figure 1.4. Generated CO_2 by combustion of fossil fuels (coal, natural gas, and oil) is captured in the first step, then, storage and transportation of captured CO_2 are carried out.

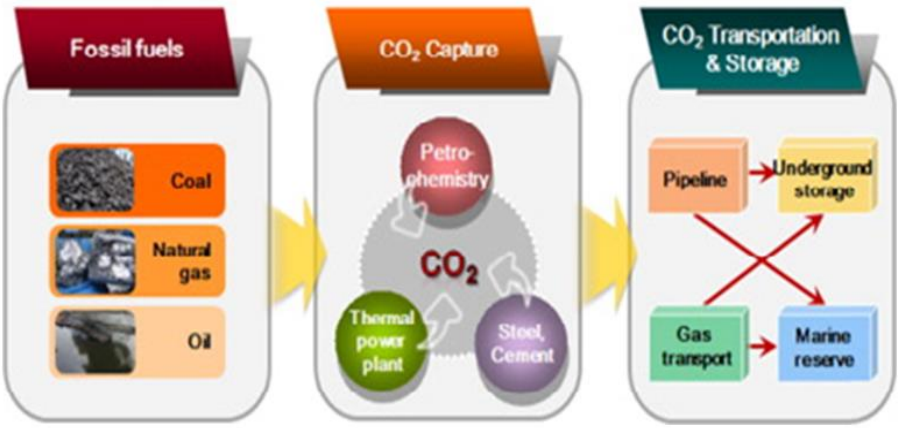

Figure 1.4. Concept of CO_2 Capture and Storage Technology. Adapted from reference 23.

Generation of power from carbon based fuel (petroleum, natural gas, and coal) is a chemical process derived from the oxidation of carbon to CO_2.[10] Unfortunately, production of CO_2 is inevitable. Emission of CO_2 can be reduced by CCS technologies commonly classified as pre-combustion, oxy-fuel combustion, and post-combustion systems depending on the concentration of CO_2 in gas stream and type of fuel.[11]

1.3.1. Pre-combustion

Pre-combustion capture includes decarbonation of gasified fuel (coal, natural gas or biomass) to produce hydrogen and carbon monoxide.[10] Fuel (C-source) is reacted with oxygen (or air) or oxygen and steam (H_2O) and hydrogen and carbon monoxide are the major components of product. Carbon monoxide reacts with steam in a catalytic reactor to form CO_2 and hydrogen, and finally CO_2 is separated from this mixture.[11] This technology is called "Integrated Gasification Combined Cycle" (IGCC) process and the reactions for the IGCC process are as given below[24]:

(1) $2C + O_2 + H_2O \rightarrow H_2 + CO + CO_2$

(2) $C + H_2O \rightarrow H_2 + CO$

(3) $CO + H_2O \rightarrow CO_2 + H_2$

Pre-combustion capture requires lower energy for CO_2 capture and it has a great potential for future use.[10] However; pre-combustion capture is a costly process for generating facilities.[11]

1.3.2. Oxy-fuel Combustion

Oxy-fuel Combustion is considered as one of the very a promising technology for capturing CO_2. Instead of air, pure oxygen that is obtained from the separation of air is used for the combustion of fuels and the fuel is burnt by this high purity oxygen to form CO_2 and water vapor.[25] The water can be removed by condensation and CO_2 can be separated easily. Even though this technique provide some cost benefits for capturing CO_2, separating oxygen from the air cause significant increase of the cost. Moreover, oxy-fuel combustion has some limitations such as the requirement of using construction materials which are resistant to high temperatures.[5]

1.3.3 Post-combustion

Post-combustion capture is a widely used process to remove CO_2 from the combustion of fuels before their emission to the atmosphere.[10] Removal of CO_2 from fossil fuel power plants is demonstrated in Figure 1.5. Air (21% O_2- 79% N_2) is used for combustion process in power plants and flue gas at atmospheric pressure is generated.[5] In post-combustion capture, produced flue gas contains CO_2 with a low pressure (approximately 1 bar) and low CO_2 content (3-20%) at high temperatures (120-180 ^oC).[26]

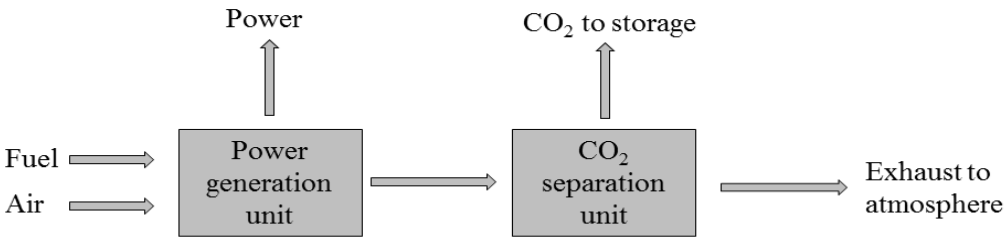

Figure 1.5. Principle of post-combustion CO_2 capture. Adapted from references 27–29.

There are several methods for capturing CO_2 by post-combustion technologies: wet absorption[30–32], membrane-based separation[33,34], dry adsorption[35–37], and cryogenics[38,39] as summarized in Figure 1.6.

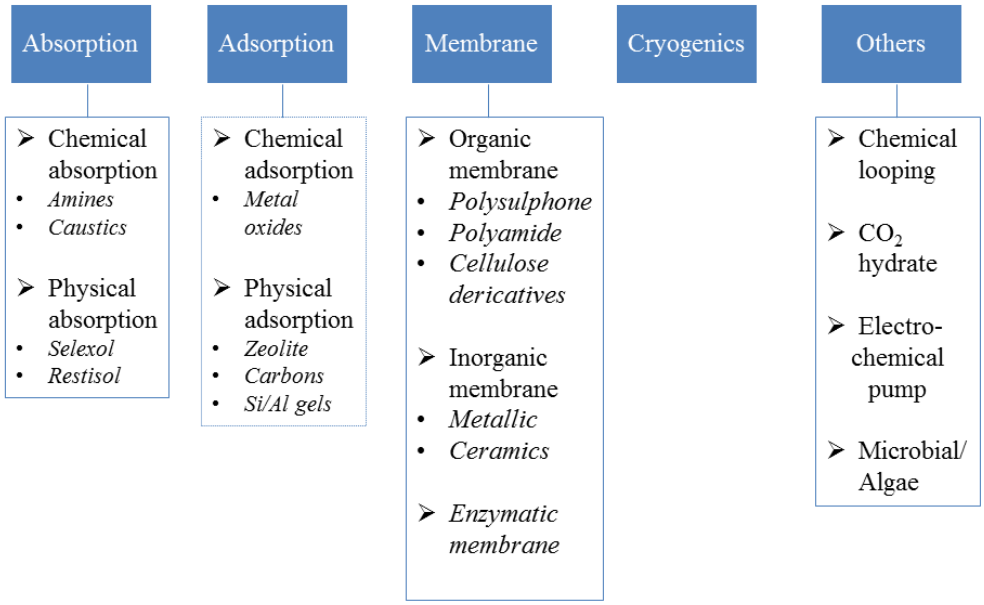

Figure 1.6. Classification of application technologies for post-combustion capture of CO_2. Adapted from reference 14.

i) Absorption method: The method include both chemical and physical absorption processes and is a widely used to capture CO_2. The method based on the reaction of the CO_2 and solvent (the aqueous solution of amines).[40–43] Absorption process has some limitations such as high regeneration cost of solvent, corrosion, implementation of gas-liquid contacting devices, etc.[5]

ii) Membrane-based separation method: This method is generally used for capturing high concentration of CO_2 from gas stream that has mainly CO_2 and CH_4 gases.[44] Membranes have semi-permeable structures acting as a filter to separate substances by solution-diffusion, adsorption-diffusion, and ionic transport.[11] Membrane process has simple molecular system and has no regeneration energy required. However, there are many disadvantages over membrane process. For instance, high degrees of separation cannot be achieved, recycling process comprise multiple stages, and membranes display sensitivity to sulphur compounds.[11]

iii) Cryogenic distillation: It is a novel technique for post combustion of CO_2 and it has been used for years to separate air into its primary components.[44] In cryogenic system, physical separation of CO_2 from other gas stream is done on the basis on sublimation.[45] Removing trace water from feed causes high cost in CO_2 capture and the phase behavior of CO_2 bring about the formation of solid plugging the equipment.[46]

iv) Adsorption: The method is based on the attachment of gas molecules onto a solid surface.[6,44] The adsorption quality is affected by the properties of adsorbate (polarity, size, and molecular weight of gas molecules) and the solid surface (pore size and polarity).[6] The adsorption process has several advantages[5]:

1- Energy requirement for adsorption process is low
2- It is easy to apply in large scale
3- Low cost

CO_2 capture by solid adsorbents is accepted as one of the most promising technology.[41] CO_2 capturing process by using dry adsorbents is a selective separation that relies on gas-solid interactions.[47] Adsorption of CO_2 on microporous solid surface (i.e. zeolite and activated carbon) that have pores which have diameter close to the gas molecules' size, occurs strongly.[48,49] The dry adsorbents such as activated carbon (carbonaceous dry adsorbent) and zeolite (non-carbonaceous dry adsorbent) are extensively used in packed columns in adsorption process due to their ease of applicability.[50] The important parameters in dry adsorption process are temperature and pressure of gas mixture, pore size of adsorbent, and surface tension of solid surface.[51]

Activated carbon is a widespread adsorbent used in industrial and technological process.[11] It has high adsorption capacity at ambient temperature and removal of moisture is not required due to the hydrophobic properties of activated carbon.[52] Activated carbon includes holes varying from micropore to macropore (Figure 1.7).[53] Even though these holes have zero-electron density, they possess intense van der Waals forces responsible for the adsorption process.[53] Activated carbon can be synthesized by using carbon-based materials such as coconut, wood, or coal.[6]

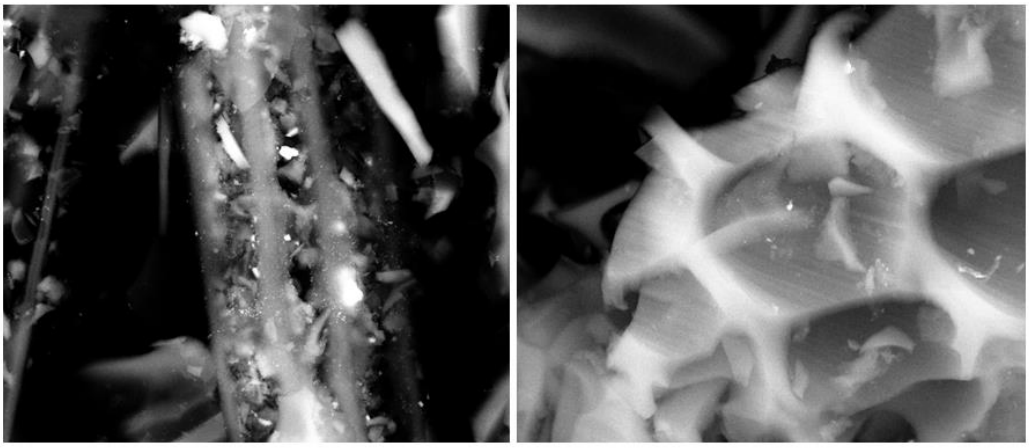

Figure 1.7. The structure of activated carbon.

The porous structure is obtained by activation processes. The activation process is applied by physically and chemically. Carbon atoms can be removed by physical (thermal) activation via carbon dioxide and water vapor at higher temperatures in order to obtain porous structure. Selective removal of carbon atoms is not successfully achieved during physical adsorption. Therefore, chemical adsorption is applied by using acids, bases, and salts to improve the yield of carbonization.[54] It includes heteroatoms (oxygen, hydroxyl and carbonyl group etc.) on their surfaces (Figure 1.8). The heteroatoms on the surface are present in form of acidic, basic, and neutral functional groups.[55] These functional groups can exist in carbonate form as a result of CO_2 adsorption. Aromatic rings have delocalized л electrons that contribute the basicity of sorbent.[56] Increase in basic character results in easier adsorption of CO_2 that have soft acidic character on surface.

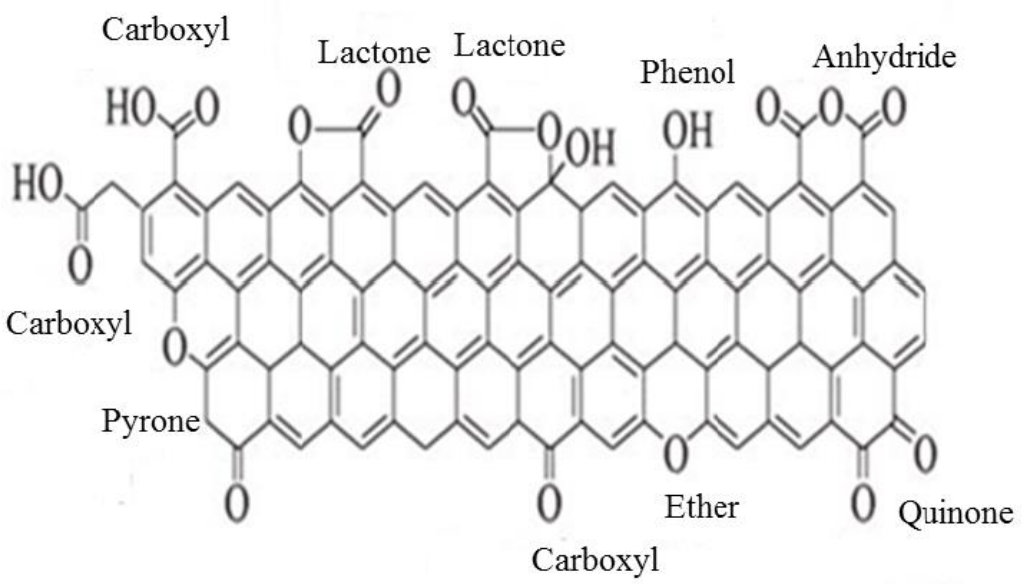

Figure 1.8. Surface chemistry of activated carbon. Adapted from reference 57.

Many studies have been conducted for activated carbon as a gas sorbent. CO_2 and N_2 separation by activated carbon for the fixed-bed adsorption at different temperatures was reported by Dantas et al.[18] A parametric analysis (radius of bed, gas temperature, heat transferred) for adsorption of CO_2 by activated carbon was carried by Saxena et al.[58] Adsorption capacity of chemically modified activated carbon improved by using acid, air oxidation, alkali impregnation, and heat treatment with He were studied by Caglayan et al.[59] Capturing of CO_2 by activated carbon prepared from biomass (gelatin and starch) was performed by Chen et al.[60]

Another very commonly used dry adsorbent is Zeolites and they are the largest group of oxide molecular sieves.[61] Zeolite has crystalline aluminosilicate framework structure containing cavities, pores, and channels for hosting ions and water molecules. (Figure 1.9) Cavities are polyhedral units that contain windows for passing of molecules in and out of cavity. Channels in the zeolite structure allow molecules to diffuse inside the pores.[62] Crystalline structure of

zeolites is formed by TO_4 (T=Si or Al) (Figure 1.9).[63] Si/Al ratio is 2.3 for Zeolite NaY.[62] Due to the porous structure of zeolite, it is widely used for separating and purifying gas molecules, in ion exchange, and in catalysis applications.[61] Separation of gas molecules is done by the help of the electrostatic interactions between CO_2 and alkali-metal cations in zeolite structure.[64] For instance, in a study conducted by Deng et al., the adsorption of SO_2, NO, CO_2 and N_2 gases at different temperatures by synthetic zeolite 13X and 5A have been reported. The amount of gases in decreasing order was reported as $SO_2 > CO_2 > NO > N_2$ based on their adsorption isotherms. [65] In another study, Chen et. al. reported that 13X zeolite have been synthesized by the hydrothermal treatment without adding extra silica and alumina sources by using bentonite. It was observed that CO_2 adsorption capacity of the zeolite increased significantly.[66]

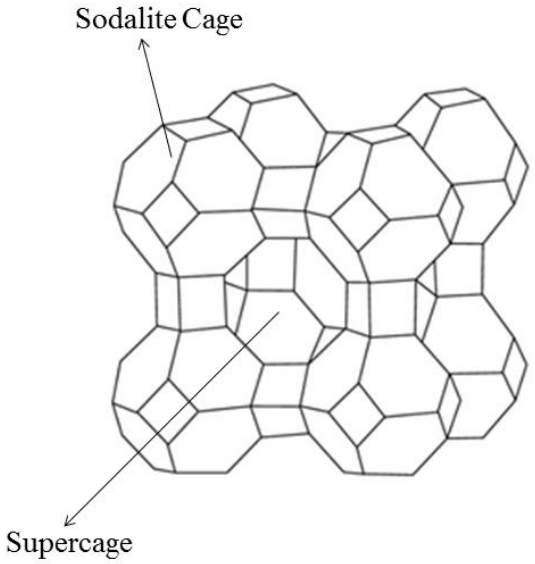

Figure 1.9. The crystalline structure of zeolite. Adapted from reference 67,68.

There are also some studies have been performed to increase CO_2 gas adsorption capabilities of dry adsorbents by implanting some metal structures and/or modifying their surface chemistry. For example, Smykowski et al. reported CO_2 adsorption on faujasite zeolite with the presence of Ir_4 clusters in the zeolite pores.[69] Another study for capturing CO_2 in low pressure is done by using both acidic and copper-exchanged SSZ-13 zeolite by Lobo et al. In this study, beside CO_2, N_2 adsorption has also been studied.[70] Moreover, LeVan et al. performed CO_2 adsorption performance on alkali metal cation (Li^+, K^+, Rb^+, and Cs^+) exchanged zeolite NaY (Na_{56} $(AlO_2)_{56}$ $(SiO_2)_{136}$. nH_2O) and NaX (Na_{86} $(AlO_2)_{86}$ $(SiO_2)_{106}$. nH_2O) . They reported that the CO_2 adsorption capacity increased for NaY zeolite in the order of Cs< Rb= K< Li= Na whereas the one on NaX zeolite increased as Cs< Rb< K< Na< Li.[63]

The use of metal oxides has also been studied as very promising alternative to dry adsorbents (i.e. zeolites and active carbon) since they have the advantage of providing selective adsorption of gas molecules. For instance, the presence of metal oxides as basic species in the medium causes preferential adhesion of CO_2 onto the metal oxide surface. They also adsorb CO_2 both chemically and physically. Chemical adsorption lead to the formation of metal carbonate and this provide an advantage of CO_2 storage more effectively.[71, 72] Studies have been conducted on CO_2 adsorption capacity of various metal oxides. For instance, the CO_2 adsorption has been performed by using metal oxides such as α-Cr_2O_3 and MgO / TiO_2.[73,74] Similarly, the CO_2 adsorption and desorption properties of copper(I) oxide and copper(II) oxide have been compared in a study by Isahak et al. Adsorption of higher amount of CO_2 by copper(II) oxide has been observed in this study.[75] The systems which include metal oxides synthesized on activated carbon the other porous adsorbent have also been studied. For example, the adsorption behavior of nickel loaded activated carbon towards CO_2 was studied by Park et al. Nickel electroless plating system which is one of the post-oxidation method, was used for producing nickel oxide layer.[76] In another study, Cu_2O on porous carbon was prepared to capture CO_2. Cu_2O

was formed by oxidizing electroplated copper film on the porous carbon surface.[77] The Cu_2O particle layer on porous carbon was reported as a very effective CO_2 adsorbing system.

The search for materials which has enhanced CO_2 adsorption capabilities lead scientist to develop new systems where nanomaterials are actively used. Nano materials having dimensions at the range of 1-100 nm have significantly high surface / volume ratio.[78] Therefore, it is expected to have increase in the amount of CO_2 adsorption with the use of appropriate materials (i.e. metal oxides) in nano-scale. The utility of various types of metal oxides nanoparticles have been investigated in CO_2 adsorption applications up to date. For instance, the adsorption ability of TiO_2, Fe_2O_3 and Al_2O_3 nanoparticles has been studied by Baltrusaitis et al.[79] Similarly, a study by Cox et al. has demonstrated improved adsorption of CO_2 gas on α-Cr_2O_3 crystals.[73] The comparison of adsorption capacity of MgO/TiO_2 mixed oxide nanoparticles and MgO or TiO_2 nanoparticles separately was done by Lee et al. and they recorded that MgO/TiO_2 mixed oxide nanoparticles have better adsorption capacity than pure MgO or TiO_2.[80]

Another route to obtain enhanced gas adsorption is to design hybrid systems where both nanomaterials and dry adsorbents are used. This has been accepted as a very promising alternative in gas adsorption technologies. Because dry adsorbents such as active carbon and zeolite, are very stable materials to host metal oxide nanoparticles for gas adsorption applications.[81] Also, existence of these particles on their surfaces contribute to the increase in surface area for adsorbing more gas molecules selectively. For example, Othman Ali et al. has reported that capturing of NO gas has been achieved by copper nanoparticles synthesized within the ZSM-5 zeolite and CuO nanoparticles formed on the zeolite external surface.[3]

The use of copper oxide nanoparticles in such hybrid system is one of the most promising way for improving gas adsorption capabilities of adsorbents such as active carbon and zeolites.[82] Copper oxide nanoparticles would contribute important advantages to the system such as having high adsorption performance at room temperature, more effective storage of CO_2 as a result of chemical interaction between copper oxide and CO_2 and requirement of low temperatures to desorb CO_2 for further use, and being cost effective.

The nanoparticles of copper oxide which are in two different oxidation state (copper(I) and copper(II)) can be used for CO_2 adsorption application. Copper(II) oxide (CuO) is p-type semiconductor and have excellent optical, electronical, physical, and magnetic properties.[83] It has narrow band gap with 1.2 eV and has monoclinic crystal system. [84] (Figure 1.10.a) Because of low cost production, nontoxic nature, good electronical and optical structure, CuO gets a great attention in some applications such as electrochemical cells, optoelectronic devices, catalysis, gas sensors besides CO_2 adsorption.[82] Copper(I) oxide (Cu_2O) is p-type semiconductor and has cubic crystal system.[1] Its band gap is 2.2 eV.[85] Cu_2O has growing interest for applications in magnetic devices[86], solar systems[87], and catalysis[88] (Figure 1.10.b)

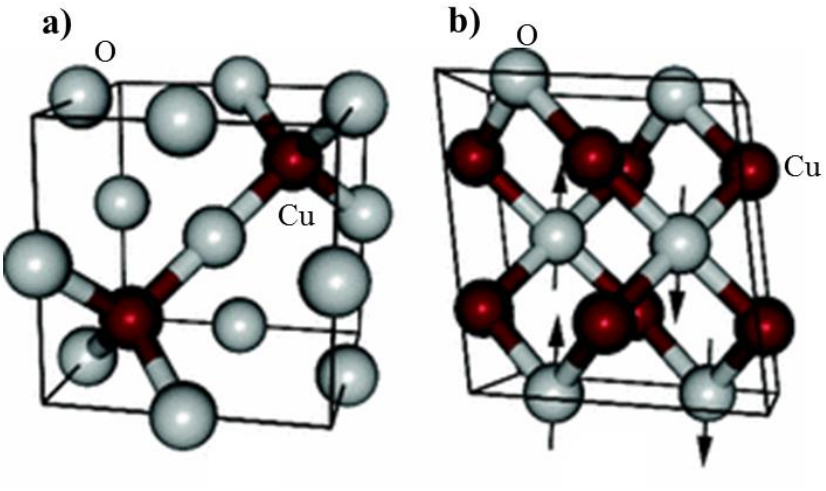

Figure 1.10. Cubic and monoclinic crystal structure of the copper oxide **(a)** Cu_2O, **(b)** CuO. Gray: copper atoms, red: oxygen atoms. Adapted from reference 89.

Copper oxide nanoparticles with basic nature attract acidic CO_2 molecules in the medium. This leads to both physical and chemical interaction between them. As a result of chemical interaction copper carbonate formation occur similar to the other metal oxides discussed above. [71,72] This provide easy storage and transformation of CO_2 and lead to potential use of copper oxides as a commercial product. [71] The advantage of copper oxides over other metal oxides for this application is the requirement of lower temperatures for both adsorption and desorption of CO_2 with the use of copper oxides. For instance, recent studies showed that calcium oxide and magnesium oxide are good at adsorbing CO_2 at 823 K and 423-673 K, respectively.[90,91] Moreover, decomposition of calcium carbonate and magnesium carbonate requires high energy (ΔH values for $CaCO_3$ and $MgCO_3$ are +178.5 kj mol^{-1} and +118 kj mol^{-1}, respectively) and it increases cost.[75] On the other hand, CO_2 adsorption on copper oxide surfaces can be achieved at room temperature and desorption of it as a result of copper carbonate can happen at ca. 583 K (ΔH values for $CuCO_3$ +45.5 kj mol^{-1}).[75]

The fabrication of a CO_2 adsorbing hybrid system with copper oxide nanoparticles firstly requires synthesis of these particles on support surfaces. There are some literature reports where Cu_2O and CuO nanoparticles have been synthesized on various support surfaces.[1,2,84,92,93] For instance, copper(I) and copper(II) oxide nanoparticles have been successfully synthesized on zeolite surface.[84,1] Copper oxide nanoparticle have loaded on activated carbon by sol-gel method for methylene blue adsorption.[94] CuO nanoparticle have been synthesis on activated multi-walled carbon nanotube for usage in super capacitor electrodes.[93] However, to best of our knowledge, there is no study reported on CO_2 adsorption on copper oxide nanoparticle encapsulated zeolites. On the other hand, there is one report discussing CO_2 adsorption on Cu_2O particle-porous carbon system.[77] Copper oxides were formed by post oxidation of copper which was electroplated on porous carbon surface.

In this thesis study, CO_2 adsorption on copper oxide (Cu_2O and CuO) nanoparticle decorated zeolite and activated carbon have been investigated. Enhancements in CO_2 adsorption upon addition of copper oxide nanoparticles on the support surfaces have been observed. The following sections of the thesis present experimental details of this investigation and discussion on findings obtained throughout the study.

CHAPTER 2

EXPERIMENTAL

2.1. Materials

Copper(II) chloride ($CuCl_2$), sodium hydroxide (NaOH), sodium chloride (NaCl), and sodium Y zeolite were purchased from Sigma Aldrich. Charcoal activated (activated carbon), sodium borohydride ($NaBH_4$) (98%), and nitric acid (HNO_3) (65%) were purchased from Merck. Deionized water was obtained by water purification system (PURELAB Option-Q, ELGA). All glassware and magnetic bars were cleaned with ethanol and distilled water and dried in an oven at 90 ^oC.

2.2. Carbon dioxide Adsorption by Copper Oxide Nanoparticles Decorated Supports

In this study, synthesis of copper oxides (Cu_2O and CuO) nanoparticles were achieved on two different supports (zeolite and activated carbon). CO_2 adsorption study was performed on copper oxide nanoparticle loaded supports. The study includes three main steps: i) pretreatment of supports, ii) synthesis of copper oxide nanoparticles on support surfaces, and iii) adsorption of CO_2 by copper oxide nanoparticle decorated supports. In the following sections, experimental details of steps for synthesis and characterization of copper oxide nanoparticles on support surfaces, and finally carbon dioxide adsorption studies are described.

2.2.1. Synthesis of Copper Oxide Nanoparticles on Zeolite Surface

2.2.1.1. Pretreatment of Zeolites

500 mg Zeolite-Y was slurried with 58.44 mg, 100 mM NaCl solution for 4 hour to remove cation sites. Slurry was washed with deionized water until the surface is free of chloride and calcined under oxygen gas at 300 ^{o}C for 12 hour in a furnace. Pretreated molecular sieves were stored under argon atmosphere.[95]

2.2.1.2. Synthesis of Cu_2O Nanoparticles on Zeolite Surface

Synthesis of zeolite framework stabilized copper(I) oxide nanoparticles was done by precipitation method.[1] Four step procedure was followed: (i) ion exchange of copper(II) chloride into the super cages of Zeolite-Y, (ii) reduction of copper ions with $NaBH_4$, (iii) calcination, (iv) oxidation by oxygen at room temperature. First, 268.9 mg $CuCl_2$ was dispersed in 20 mL water. 500 mg pretreated Zeolite-Y was added to this solution and mixed for 72 hour at room temperature. Slurry was washed three times with 20 mL distilled water and separated by centrifuging. Remnant was dried under vacuum at 90 ^{o}C. Then 1.37 M, 100 ml $NaBH_4$ was added to Cu-exchanged zeolite to reduce Cu(II) ions to Cu(0) in the reaction below:

$$BH_4^-{}_{(aq)} + 3H_2O_{(aq)} \rightarrow B(OH)_{3(aq)} + 7H^+{}_{(aq)} + 8e^-$$
$$Cu^{2+}{}_{(aq)} + 2e^- \rightarrow Cu^o{}_{(aq)}$$

The overall reaction:

$$BH_4^-{}_{(aq)} + 3H_2O_{(aq)} + 4Cu^{2+}{}_{(aq)} \rightarrow B(OH)_{3(aq)} + 7H^+{}_{(aq)} + 4\ Cu^o{}_{(aq)}$$

Mixing was continued for two minutes to let all hydrogen gas be removed. Brown precipitate formation was observed. The precipitate was separated by

centrifuging and washed with 20 mL distilled water. Next, the remnant was dehydrated in oven for 4 hours at 300 ^{o}C under vacuum. Finally, Copper(0) nanoparticles were oxidized by O_2 flow to obtain Cu_2O nanoparticles. The zeolite encapsulated Cu_2O nanoparticles were stored under argon atmosphere until further use.

2.2.1.3. Synthesis of CuO Nanoparticles on Zeolite Surface

Synthesis of zeolite stabilized CuO nanoparticles was synthesized by precipitation method. Three step procedure was followed; (i) implanting copper(II) ions into the super cages of Zeolite-Y by ion exchange (ii) precipitation of copper ions with sodium hydroxide (iii) calcination.[84] In the first step, 0.1 M (268.9 mg $CuCl_2$ in 20 mL water) $CuCl_2$ solution and 500 mg Zeolite-Y were mixed for 72 hour at room temperature with magnetic bar. Slurry was washed three times with 20 mL distilled water and separated by centrifuging. Remnant was dried in vacuum at 90 ^{o}C. Next, 20 mL of 0.1 M NaOH was added to the Cu (II) implanted zeolite to form Cu $(OH)_2$. After 2 hour reflux, black precipitate was formed. The solid was separated and washed three times with 20 mL deionized water. In the final step, the product was calcined at 350 ^{o}C for 4 hours leading to the formation of CuO nanoparticles on zeolite surface.[83] Then, zeolite encapsulated CuO nanoparticles were stored under argon atmosphere.

2.2.2. Synthesis of Copper Oxide Nanoparticles on Activated Carbon

2.2.2.1. Acid Pretreatment of Activated Carbon

Acidic pretreatment was done for activated carbon to make the surface of activated carbon more acidic. It increases the load of copper oxide nanoparticles having basic character with the help of the acid-base interaction.

5 g activated carbon was refluxed in 50 mL of 6 M HNO_3 for 1 hour at 80 ^oC. Then, activated carbon was washed three times with 20 mL distilled water and dried in oven for 2 hour at 60 ^oC under vacuum.[96] Finally, pretreated activated carbon was stored under argon atmosphere.

2.2.2.2. Synthesis of Cu_2O Nanoparticles on Activated Carbon

Synthesis of copper(I) oxide nanoparticles on activated carbon was done by precipitation method as described in the synthesis on the zeolite surface.[1] Similarly, four step procedures were followed: (i) introducing of copper(II) chloride into activated carbon, (ii) precipitation of copper ions with sodium borohydride, (iii) calcination, and (iv) oxidation by oxygen at room temperature. Firstly, 289 mg $CuCl_2$ in 20 mL water (0.1 M) and 1 g activated carbon were mixed for 17 hour at room temperature. The slurry was filtered and washed three times with 20 mL distilled water. Remnant was dried in vacuum at 90 ^oC. Next, 100 mL of 0.933 M $NaBH_4$ was added to dry solid to reduce Cu^{2+} ions to Cu (0). Mixing was continued until no more hydrogen gas evolution happen. The solid part was separated by centrifuging and washed with 20 mL distilled water. The remnant was dehydrated in oven for 4 hours at 200 ^oC under vacuum. Finally, copper(0) nanoparticles are oxidized by O_2 to form copper(I) oxide nanoparticles. Activated carbon with Cu_2O nanoparticles was stored under argon atmosphere.

2.2.2.3. Synthesis of CuO Nanoparticles on Activated Carbon

Synthesis of CuO nanoparticles on activated carbon was also done by precipitation method.[83] Similar to the synthesis on zeolites, here too, three step procedure was followed: (i) Introducing copper(II) chloride into activated

carbon, (ii) precipitation of copper ions with $NaBH_4$, (iii) calcination. In the first step, 289 mg $CuCl_2$ in 20 mL water (0.1 M) and 1 g activated carbon were mixed for 17 hours at room temperature. Then, slurry was washed three times with 20 mL distilled water and separated by centrifuging. Remnant was dried in vacuum at 90 ^oC. Next, 20 mL of 0.1 M NaOH was added to the Cu(II) exchanged activated carbon to form $Cu(OH)_2$. After 2 hour reflux, black precipitate was collected. The solid was separated and washed three times with 20 mL distilled water. The product was dried for 16 hour at 80 ^oC and finally calcined at 350 ^oC for 4 hours. CuO nanoparticles loaded on activated carbon were stored under argon atmosphere.

2.2.3. Carbon Dioxide Adsorption Studies

Qualitative analysis of CO_2 adsorption on Cu_2O and CuO nanoparticles decorated activated carbon and zeolite were performed by using a setup shown in Figure 2.1. Before adsorption studies, copper oxide (Cu_2O and CuO) nanoparticle containing adsorbents (activated carbon and zeolite) were degassed at 423 K for 2 hours. 0.5 g of solid adsorbent was used in each experiment. Experiments were performed under gas mixture of 5 % CO_2 and 95 % N_2 with flow rate of 10 mL/min. Before flowing CO_2 gas through the samples, Ar gas was passed to make the atmosphere inside the glass column inert. CO_2 was exposed on adsorbents surfaces for 2 hours.

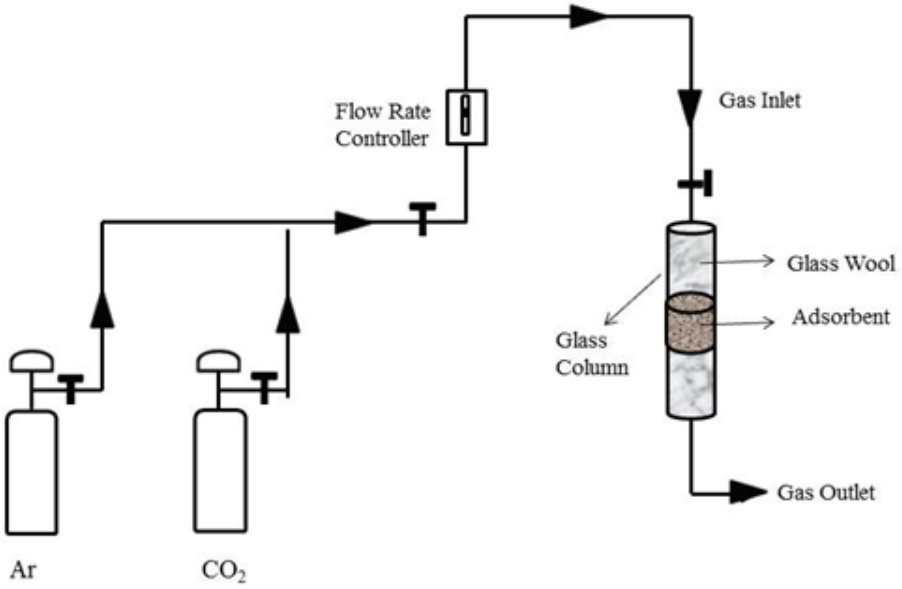

Figure 2.1. Schematic diagram of CO_2 adsorption set-up for qualitative analysis.

FTIR analysis for CO_2 gas, adsorbed CO_2 by supports (activated carbon and zeolite) and supports with Cu_2O and CuO nanoparticles were studied by the set-up represents in Figure 2.2. Samples are degassed at 423 K for 2 hours. 0.3 g adsorbents are used for each set. Experiments were performed under gas mixture of 5 % CO_2 and 95 % N_2 with flow rate of 1 mL/min. CO_2 and N_2 gas mixture was used as references. After passing the mixture through the gas cell for each set, pure N_2 gas with flow rate 1 mL/min was used for cleaning the gas cell. The FTIR spectrum was taken in every 5 minutes.

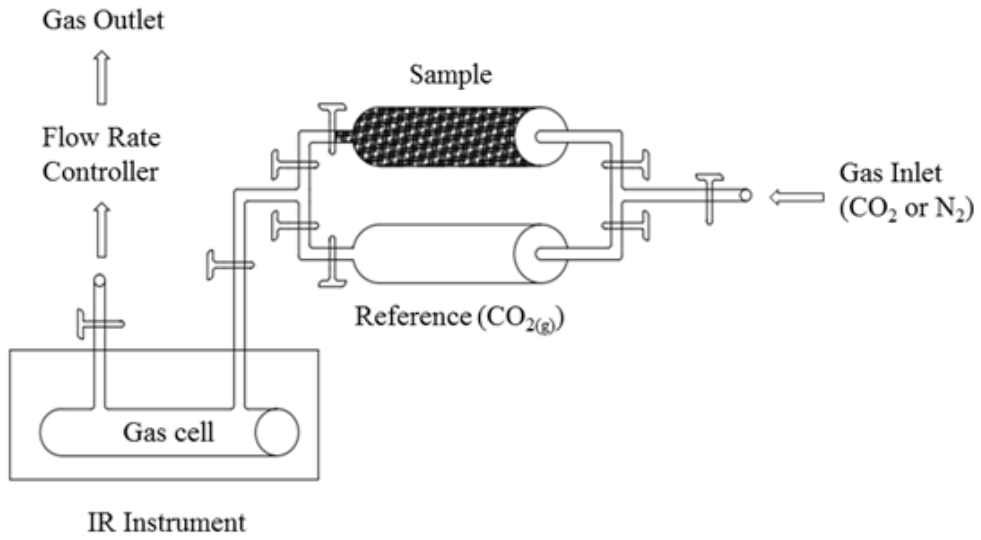

Figure 2.2. Schematic diagram of CO_2 adsorption set-up for analysis of adsorbed CO_2 via FTIR spectroscopy.

2.3. Transmission Electron Microscopy (TEM)

The morphologies of Cu_2O and CuO nanoparticles on adsorbents (zeolite and activated carbon) surfaces were investigated via JEM 2100F-RTEM analysis. TEM sample preparation was performed by suspending copper oxide nanoparticles containing support powders in ethanol. After the suspension was stirred in an ultrasonic bath, an aliquot was dropped onto copper grid. It was waited for overnight to dry.

2.4. Scanning Electron Microscopy (SEM)

QUANTA 400F Field Emission SEM instrument was also used for characterization of nanoparticles on support surfaces.

2.5. X-Ray Diffraction (XRD)

The crystallinity of both nanoparticle containing adsorbents and bare-adsorbents were analyzed by using Rigaku MiniFlex X-ray Diffractometer with X-ray radiation source Cu Kα. 2δ diffraction angle from 10^o to 80^o with a scan speed 1 ^{o}/min. 0.2 g sample was used in each analysis.

2.6. X-Ray Photoelectron Spectroscopy (XPS)

The surface analysis of activated carbon, zeolite, and copper loaded adsorbents were performed on ESCA-XPS with monochromatic Al Kα radiation, 27.1 W, 58.70 eV, and 45.0 ^{o}. C1s of 284.5 eV was taken as a reference.

2.7. Fourier Transform Infrared (FTIR) Spectroscopy

Copper oxide nanoparticles on supports and carbonate formation after CO_2 treatment were characterized by Nicolet 6700 FTIR instrument with IR source and MCT/A detector. IR pellets were prepared by dispersing 2 % (by weight) of activated carbon and 5 % (by weight) zeolite based samples in KBr matrix.

2.8. Thermo gravimetric Analysis (TGA)

Thermo gravimetric analyses for activated carbon and zeolite were conducted on Perkin Elmer Pyris 1 TGA equipment. 5±0.2 mg of each sample was used in each analysis. All TGA samples were waited at 323 K for 5 min to minimize difference in moisture content between all samples. Then, all samples were heated up to 973 K at a rate of 278 K/min with a nitrogen flow rate of 20 mL/min.

2.9. Brunauer-Emmett-Teller Analysis (BET)

Physical surface analysis was performed with Quantachrome Coporation, Autosorb-6 BET instrument. Surface area and micropore volume micropore area were calculated from the adsorption isotherms. Samples were dehydrated at 623 K for 6 hours before each analysis.

CHAPTER 3

RESULTS & DISCUSSION

3.1. Synthesis and Characterization of Copper(I) Oxide (Cu_2O) Nanoparticles on Activated Carbon and Zeolite Surfaces

The synthesis of Cu_2O nanoparticles on zeolite and activated carbon surfaces were achieved with a precipitation method as described in literature.[84, 1] The first step of the method involve introduction of Cu^{2+} ions on pretreated support surface via ion exchange. Then reduction of Cu^{2+} to copper(0) and was done by $NaBH_4$ to form copper(0) particles. Finally copper(0) nanoparticles were oxidized by O_2 treatment to form copper(I) oxide (Cu_2O) nanoparticles.

Figure 3.1 shows the SEM images of bare activated carbon support and Cu_2O nanoparticles synthesized on this support. The SEM images demonstrate Cu_2O nanoparticles are well dispersed on activated carbon surface. Agglomeration were not observed. The avarage sizes of Cu_2O nanoparticles on activated carbon surfaces are 45 ± 5 nm with spherical-like shape. Figure 3.1.f shows the EDX spectrum of Cu_2O nanoparticles on activated carbon surfaces, suggesting the presence of copper and oxygen in the sample.

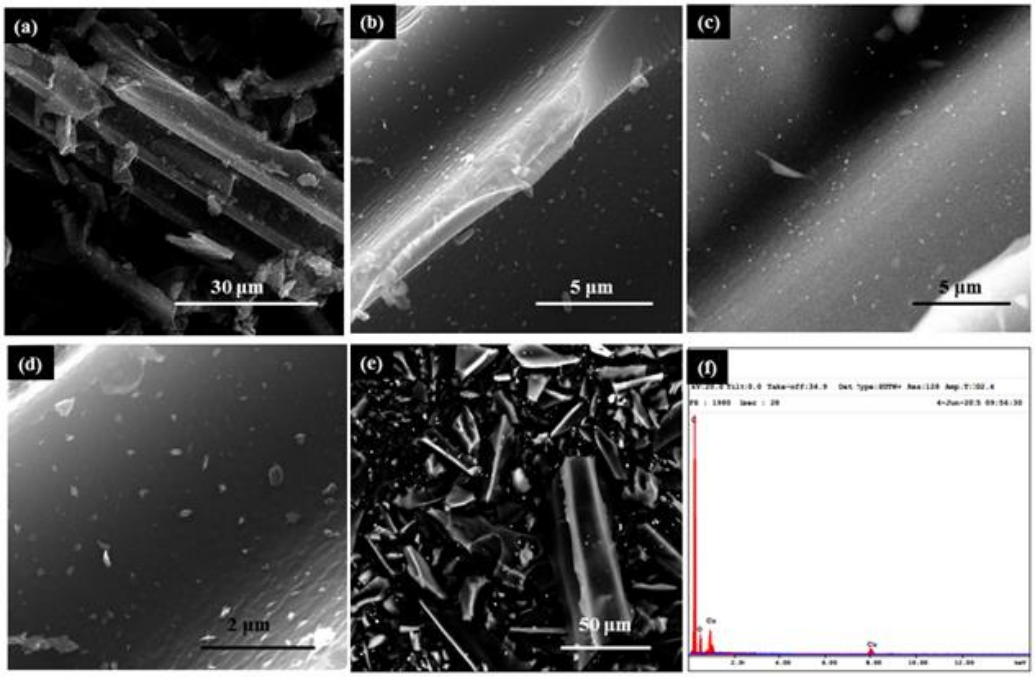

Figure 3.1. (a) SEM image of activated carbon, **(b-d)** SEM images of Cu_2O nanoparticles on activated carbon at different magnification, **(e)** back-scattered SEM images of Cu_2O nanoparticles on activated carbon **(f)** EDX of Cu_2O nanoparticles on activated carbon. (Wt % :C (81.84), O (12.65), Cu (5.50)).

SEM images of Cu_2O nanoparticles synthesized on zeolite surfaces and bare zeolites are demonstrated in Figure 3.2. The avarage sizes of Cu_2O nanoparticles on zeolite surfaces are 45 ± 5 nm with spherical-like morphology. Eventhough the dispertion of nanoparticles on zeolite surface is mostly well, some agglomeration of the nanoparticles was also observed. The EDX analysis of Cu_2O nanoparticles on zeolite surface suggests the presence of copper oxide nanoparticles on zeolite surfaces (Figure 3.2.f). The observed Na, Al, and Si peaks belong to the zeolite.

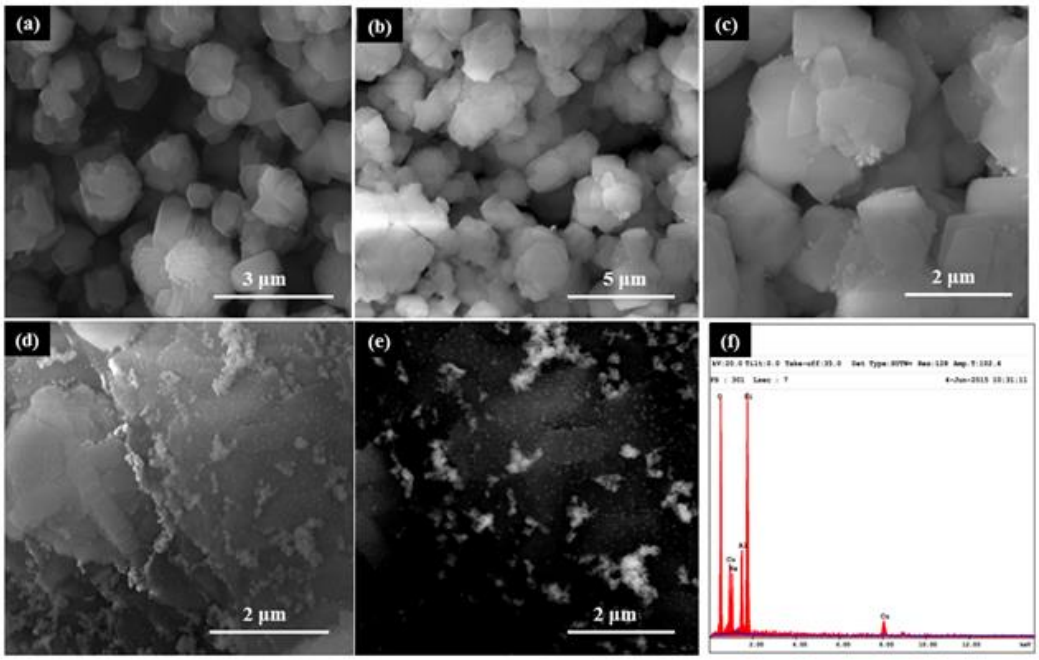

Figure 3.2. (a) SEM images of zeolite **(b-d)** SEM images of Cu_2O nanoparticles on zeolite surface at different magnification, **(e)** back scattered SEM image of Cu_2O nanoparticles on zeolite **(f)** EDX of Cu_2O nanoparticles on zeolite surface (Wt % :O (41.69), Na (9.65), Al (9.62), Si (28.85), Cu (10.20)).

TEM analysis was performed to better analyze the morphology of nanoparticles and their dispersion on the support surface. The TEM images of zeolite and copper(I) oxide on zeolite surfaces show that Cu_2O nanoparticles have spherical-like shape with average sizes of 45 ± 5 nm. This observation agree with the one in SEM analysis. (Figure 3.3) The TEM images also demonstrate that significant amount of Cu_2O nanoparticles are placed on zeolite surfaces in well dispersed form.

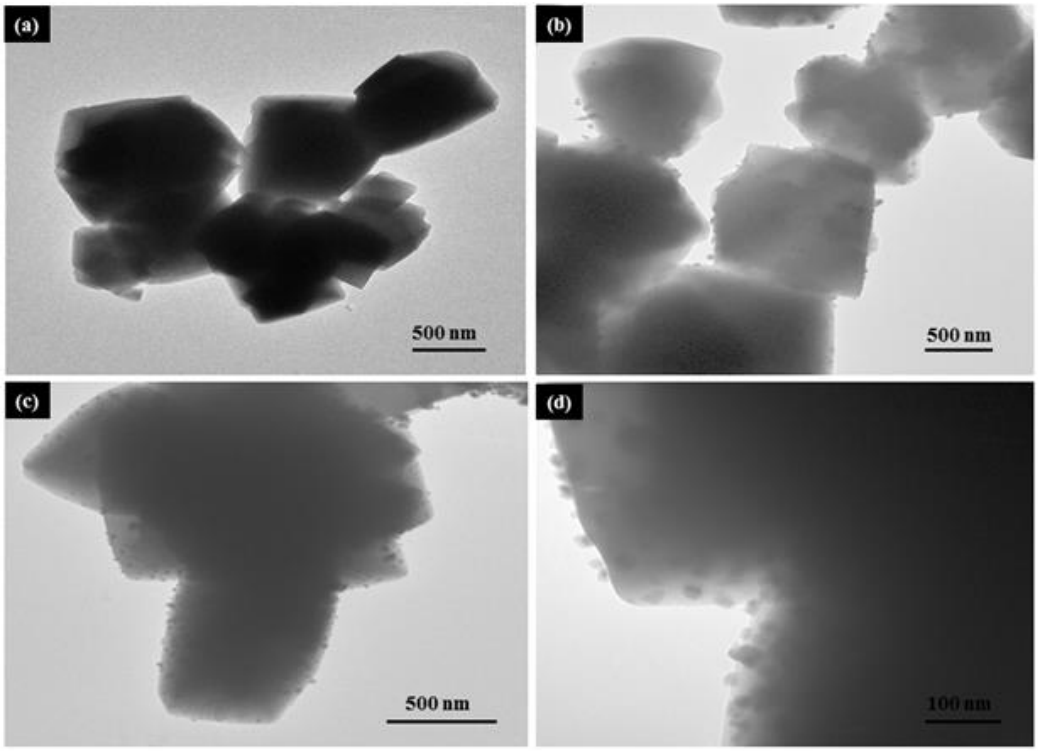

Figure 3.3. (a) TEM image of zeolite, **(b)-(d)** TEM images of Cu_2O nanoparticles within zeolite at different magnifications.

XRD study was performed to investigate the crystallinity of the prepared system. Figure 3.4 shows the XRD patterns of activated carbon and Cu_2O nanoparticles on activated carbon. Comparison of these patterns shows no observable difference and Cu_2O signature peak which is expected to be at 36.5^{o} [1] was not observed in the XRD spectrum of the Cu_2O nanoparticle-activated carbon system. This is most likely due to existence of significantly lower amount of Cu_2O nanoparticles on activated carbon surface compared to the one of activated carbon as a host material. This might be because activated carbon surface can not hold the copper ions efficiently in the initial step of the synthesis procedure, thus the amount of nanoparticles synthesized on the surface decrease.

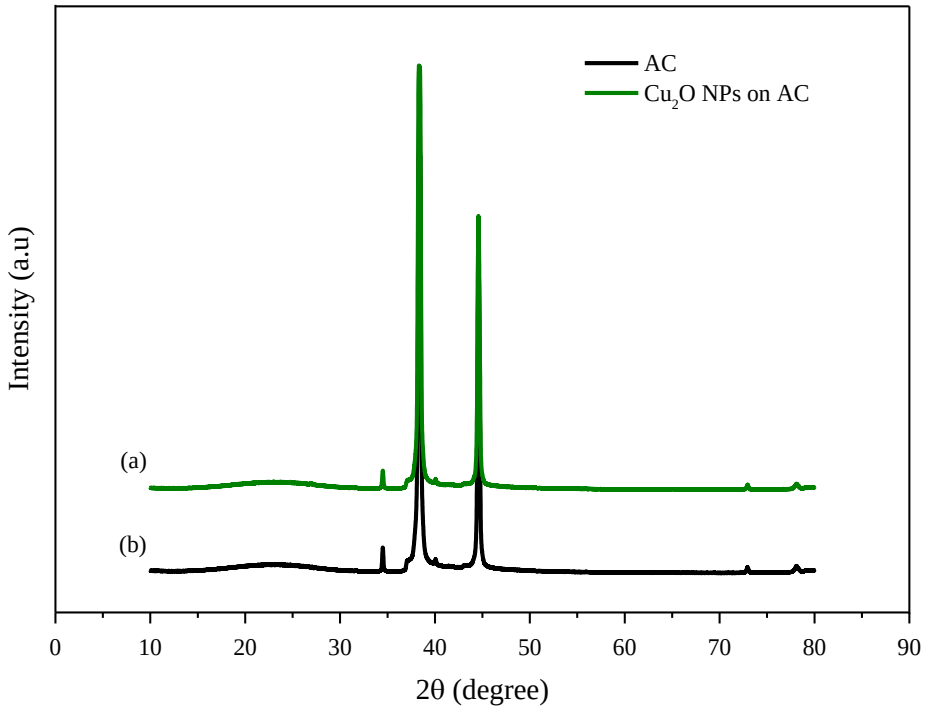

Figure 3.4. XRD patterns of **(a)** activated carbon (AC) **(b)** Cu_2O nanoparticles (NPs) on activated carbon.

XRD pattern of zeolite and Cu_2O nanoparticles on zeolite surface are given in Figure 3.5. The presence of two peaks at 35.57^o and 38.04^o confirm the formation of Cu_2O nanoparticles on zeolite surface.[97] Low intensity of these peaks imply the low loading of the nanoparticles on zeolite surface similar to the synthesis on activated carbon. Comparison of the XRD patterns shows that crystalline form of zeolite support did not change after the Cu_2O nanoparticles synthesis on its surface.

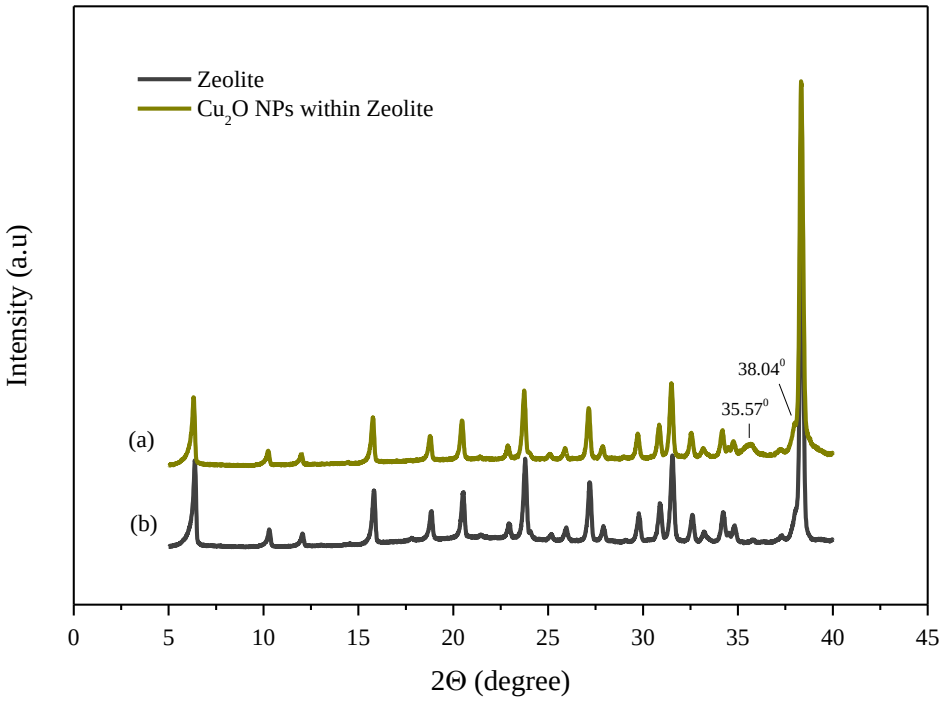

Figure 3.5. XRD patterns of (a) zeolite (b) Cu_2O nanoparticles within zeolite.

XPS studies were performed for copper(I) oxide (Cu_2O) nanoparticles loaded on activated carbon and zeolite. (Appendix Figure A1-3) The full XPS spectra of both hybrid systems are shown in Appendix Figure A1 and A2. The each spectrum demonstrates strong peaks of carbon and oxygen as well as the weak ones of copper. The low intensity of copper peaks most likely because of the low copper content on the support surface. (Figure A.1.c and A.2.c) Similar to the observations in previous literature reports,[96] here too, the detection of copper in the pores of support was hampered since XPS is a surface characterization technique. Even though the collected spectra did not provide enough clues to estimate the oxidation state of copper, it was helpful to verify the presence of copper in both hybrid systems.

3.2. Synthesis and Characterization of Copper(II) Oxide (CuO) Nanoparticles on Activated Carbon and Zeolite Surfaces

CuO nanoparticles were synthesized by precipitation method as described in literature.[1,83,84] Briefly, mixing copper precursor and supports (activated carbon or zeolite) was followed by the addition of NaOH to form $Cu(OH)_2$. Dehydration of the precipitate resulted in the formation of CuO nanoparticles on supports' surface.

SEM images of activated carbon and CuO nanoparticles on activated carbon are shown on Figure 3.6. The SEM analysis demonstrate that the CuO nanoparticles are well dispersed and did not agglomarate on activated carbon surface. The CuO nanoparticles have the average sizes of 60 ± 5 nm and needle-like morphologies. The EDX spectrum shows copper peaks suggesting the existence of copper nanoparticles on activated carbon surface. (Figure 3.6. f)

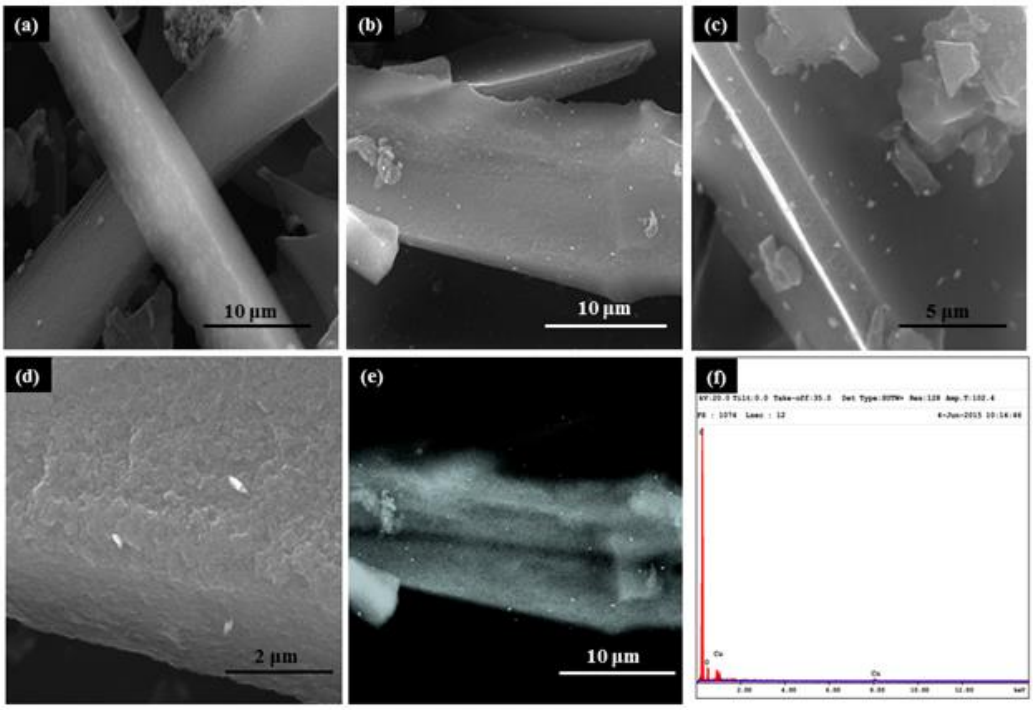

Figure 3.6. (a-d) SEM images of CuO nanoparticles on activated carbon at different magnification, **(e)** back-scattered SEM images of CuO nanoparticles on activated carbon **(f)** EDX of CuO nanoparticles on activated carbon (Wt % :C (88.64, O (9.15), Cu (2.20)).

CuO nanoparticles synthesized on zeolite surface have spiky morphologies. (Figure 3.7) The SEM analysis show that the CuO nanoparticles present on zeolite surface in well dispersed fashion. EDX spectrum show peaks verifying the existence of CuO nanoparticles on zeolite surface as well as the ones of zeolite. (Figure 3.7.f).

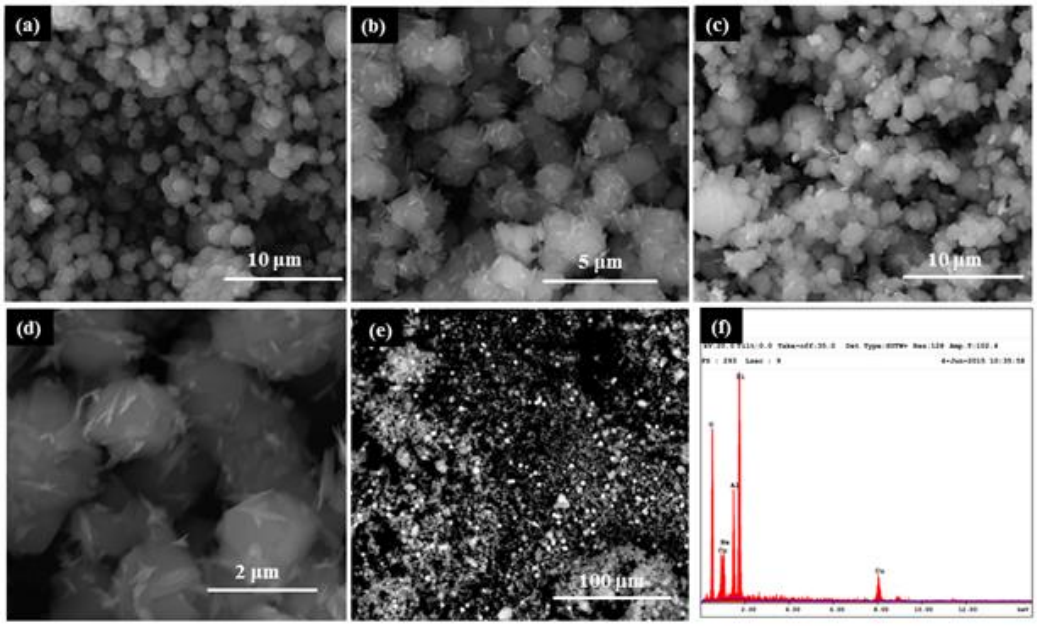

Figure 3.7. (a) SEM images of zeolite, **(b-e)** SEM images of CuO nanoparticles within zeolite at different magnification, **(f)** EDX of CuO nanoparticles within zeolite (Wt % :O (40.41), Na (8.62), Al (9.73), Si (25.11), Cu (16.11)).

The TEM images of zeolite without and with CuO nanoparticles are given in Figure 3.8. In Figure 3.8.a shows the zeolite structure which has hexagonal shape and channels. TEM analysis demonstrate that CuO nanoparticles assembled out from the zeolite surface irregularly to form spiky-like structures.CuO nanoparticles constructing these assemblies have sizes of 10 ± 5 nm

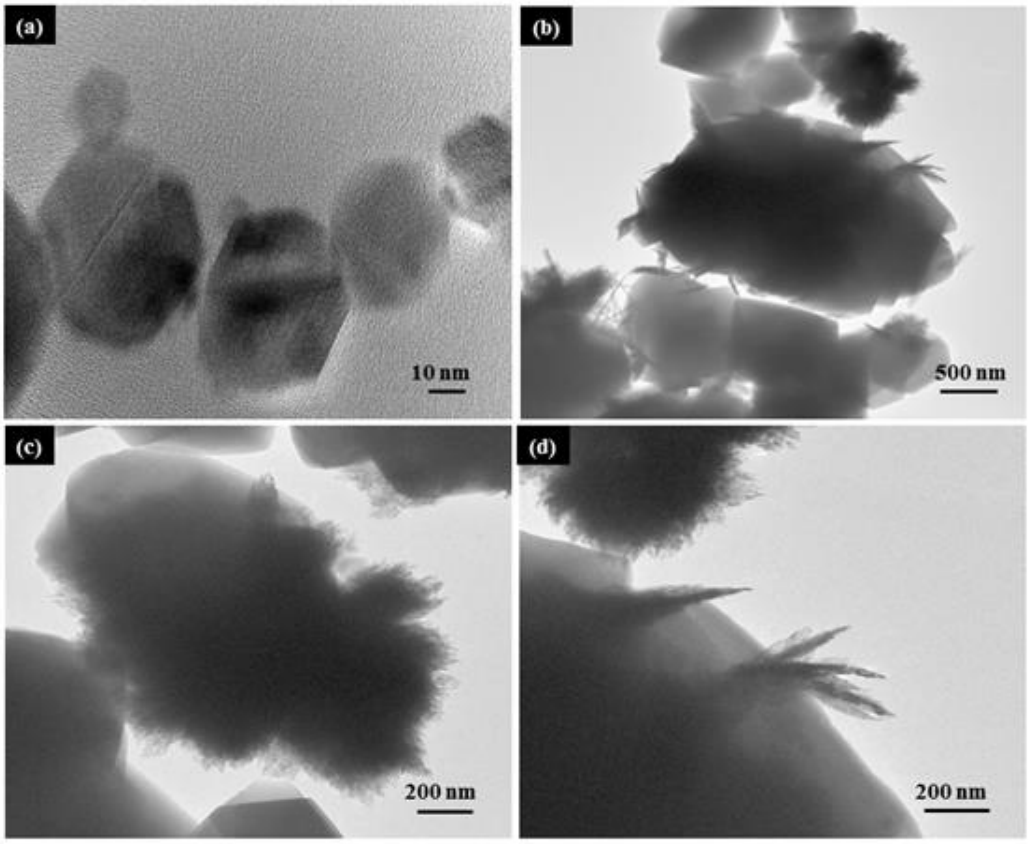

Figure 3.8. (a) High resolution TEM image of zeolite, **(b-d)** TEM images of CuO on zeolite surface at different magnifications.

XRD pattern of activated carbon and CuO loaded activated carbon are given in Figure 3.9. The peak at 35.75^{o} confirms the presence of CuO in the copper oxide-activated carbon hybrid system. Similar to the XRD analysis of Cu_2O on supports, here too, no other CuO peak was observed. As it was explained in the previous section, the most likely reason was considered as the inefficient loading of copper ions on support surface and thus formation of fewer nanoparticles on it. Comparison of the XRD spectrum of activated carbon supported Cu_2O and CuO nanoparticles suggest that CuO nanoparticle exist in higher amount on support surface. This lead to relatively more clear observation of CuO peaks in the detection limits of the XRD analysis.

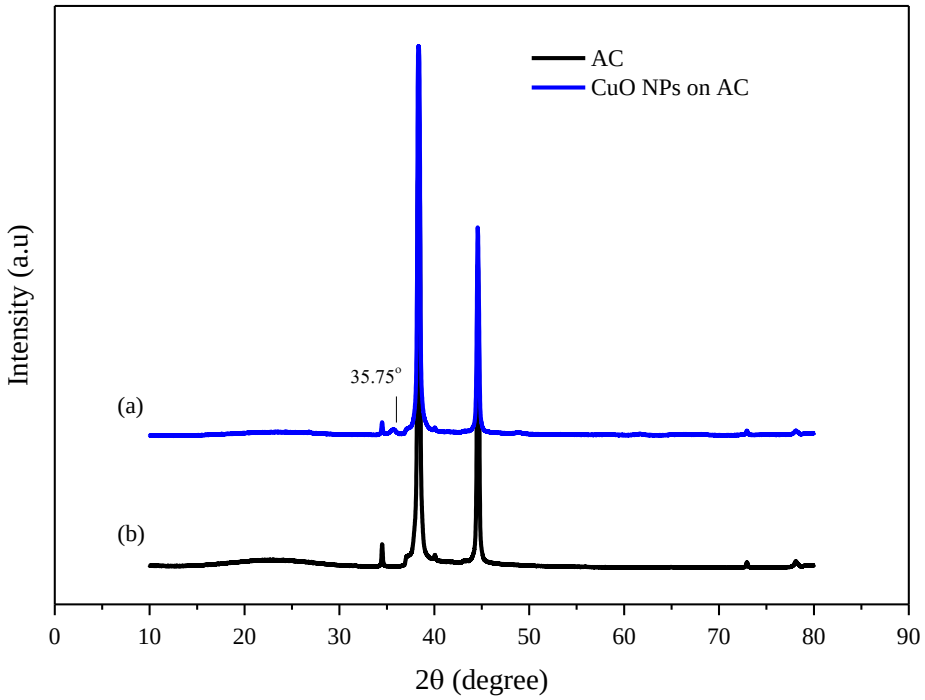

Figure 3.9. XRD patterns of **(a)** activated carbon (AC) **(b)** CuO nanoparticles (NPs) on activated carbon.

XRD spectrum of zeolite and zeolite supported CuO nanoparticles are given in Figure 3.10. As in the activated carbon system, one of the signature peak (at 35.48^{o}) of CuO is clearly seen in the spectra of CuO nanoparticles synthesized on zeolite surface, too. The low intensity of this peak suggest the existence of low amount of CuO on zeolite. Observing the zeolite peaks (at 32.58^{o}, 38.97^{o}, 48.74^{o})[83] in both spectrum unchanged show that the zeolite framework and its crystalline nature remined after CuO synthesis on it.

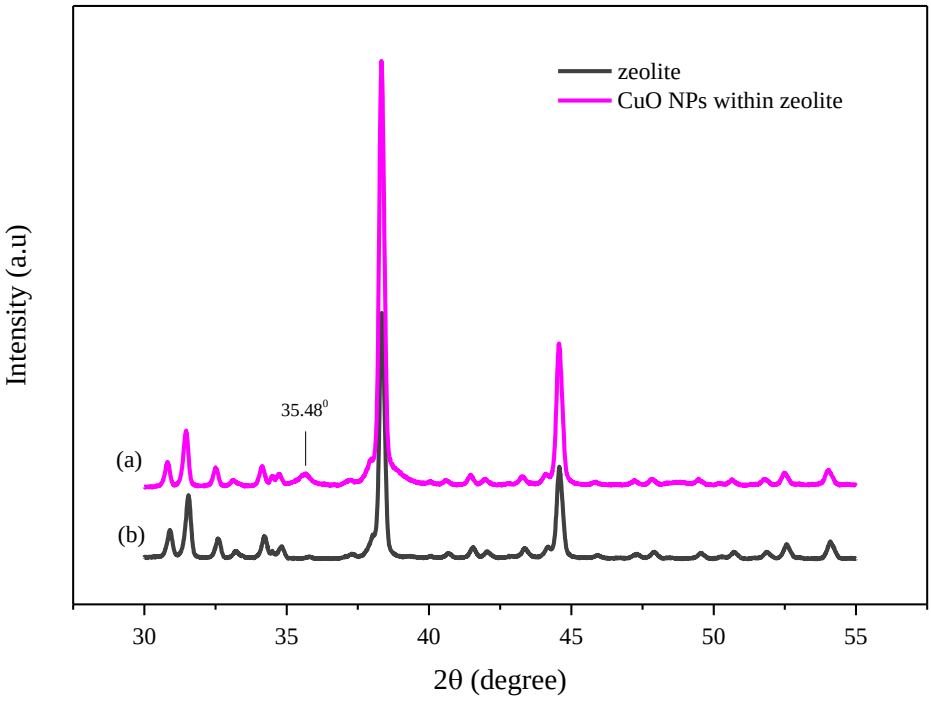

Figure 3.10. XRD patterns of **(a)** Zeolite and **(b)** CuO nanoparticles (NPs) on zeolite surface.

The composition of CuO nanoparticles on zeolite hybrid system was examined by XPS analysis. (Figure 3.11 and 3.12) The survey XPS spectrum suggests the presence of copper on zeolite surface as well as the presence of Na, Si, Al, and O which belong to zeolite structure. (Figure 3.11) No other contaminant species were observed except C1s which is used as a reference.

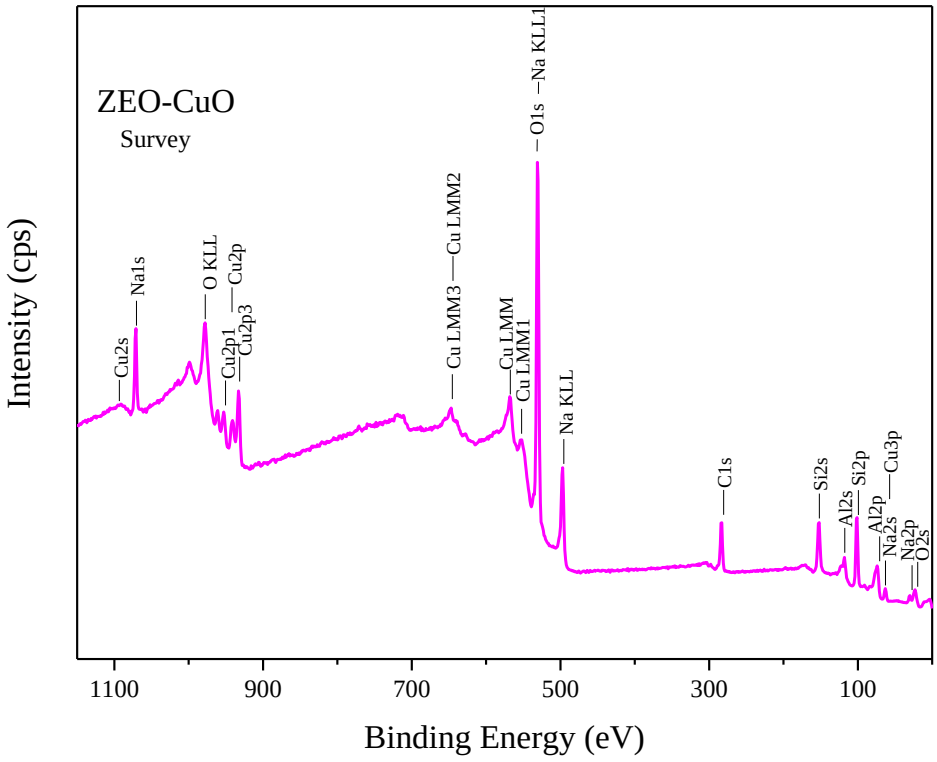

Figure 3.11. The XPS survey spectrum of zeolite with CuO**.**

A C1s spectrum is given in Figure 3.12. a. The spectrum shows a C 1s peak position at 283.41 eV. This peak is shifted 1.19 eV toward lower binding energy relative to the reference value for C1s is 284.6 eV. This is most likely because of the matrix effect of Na-Zeolite Y. The C1s peak was used to calibrate the collected spectra. A O1s spectrum is given in Figure 3.12. b. Two peaks were observed at 530.8 eV and 528.3 eV with a difference 2.5 eV which is similar to the reference value 2.1 eV.[98] The peak located at 528.3 eV indicates the O^{-2} in CuO. The other peak suggests the adsorbed O on CuO surface. The presence of significant amount of copper oxide nanoparticle assembly on zeolite surface led clear identification of copper oxide type by this technique. The XPS spectrum shows sharper signals of copper for CuO-zeolite system compared to the one of Cu_2O – zeolite/active carbon. (Figure 3.12.c) Cu $2p_{1/2}$ and Cu $2p_{3/2}$ peaks are observed at 952.1 eV and 932.2 eV, respectively. The binding energy difference between two peaks is 19.9 eV. Cu $2p_{1/2}$ and Cu $2p_{3/2}$ peaks have been previously reported as 954.3 eV and 934.3 eV, respectively for as-synthesized CuO

powders.[99] The peak positions and the difference between them observed in this thesis study agree well with the previously reported literature values. Therefore, the presence of CuO nanoparticles on zeolite surface is suggested based on this comparison. . Moreover, strong satellites peaks were observed in Cu2p core level XPS spectrum. The first satellite peak located at 961 eV was appeared in higher energy side of Cu $2p_{1/2}$ (952.1 eV) and the difference was about 8.9 eV. The other strong satellites were located between Cu $2p_{1/2}$ and Cu $2p_{3/2}$ peaks. These satellites peaks suggests the presence of CuO due to the having d^9 configuration in ground state.[100–102]

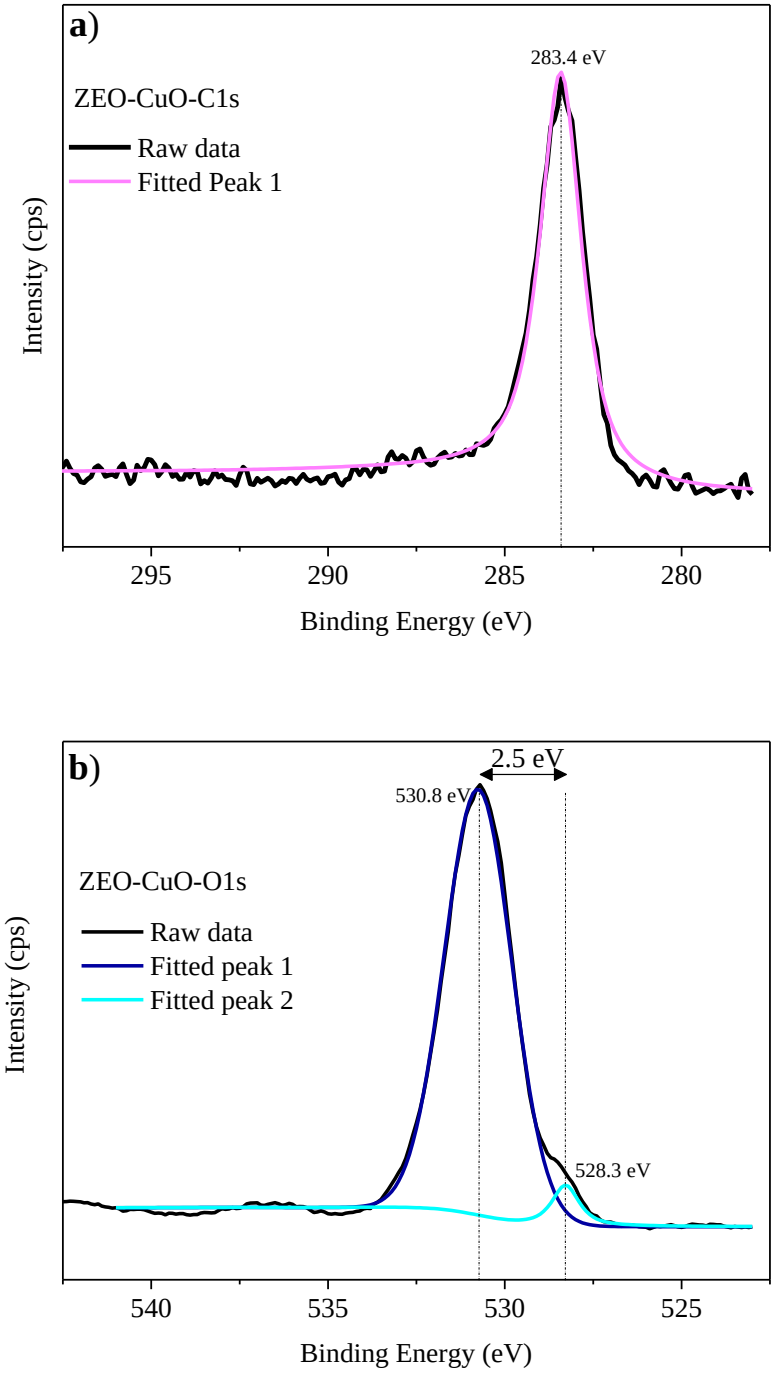

Figure 3.12. The XPS spectra of zeolite with CuO a) C1s, b) O1s c) Cu2p.

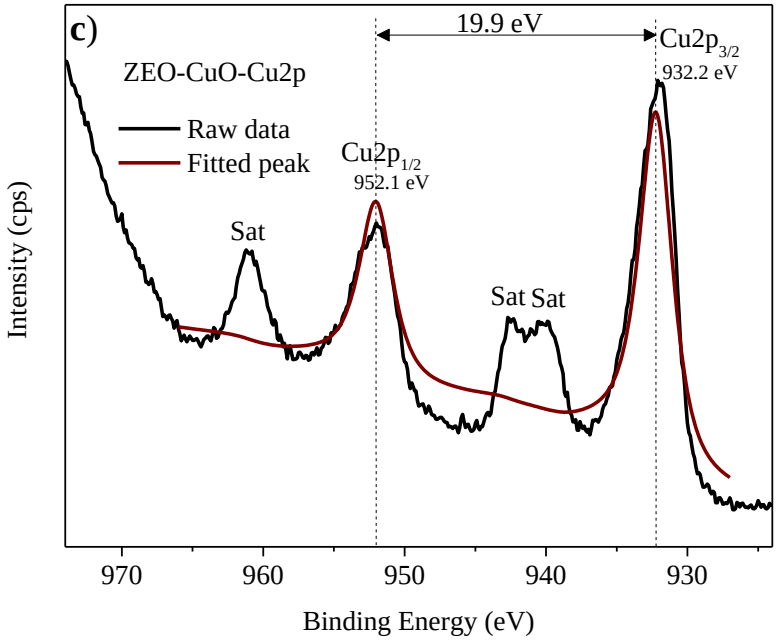

Figure 3.12. The XPS spectra of zeolite with CuO **a)** C1s, **b)** O1s **c)** Cu2p. (continued)

XPS analysis was also performed for CuO nanoparticle-active carbon system. (Appendix Figure A.1) The XPS spectrum shows strong peaks of carbon and oxygen, and weak ones of copper similar to the spectra of Cu_2O nanoparticle-zeolite/active carbon systems. (Figure A.2 and A.3) As it was noted in the previous section, the reason for this observation is considered as the low amount of copper nanoparticles on support surface. Therefore, clear identification of copper oxidation state could not be done. On the other hand, observation of copper signals proves the existence of copper on zeolite surface.

3.3 Characterization of Surface Area and Pore Volume of Activated Carbon and Zeolite Supported Copper Oxide Nanoparticles

Nitrogen adsorption-desorption isotherms of activated carbon and copper oxide nanoparticle loaded activated carbon are given in Figure 3.13 and all show Type I shape that is a characteristic of microporous materials.[103]

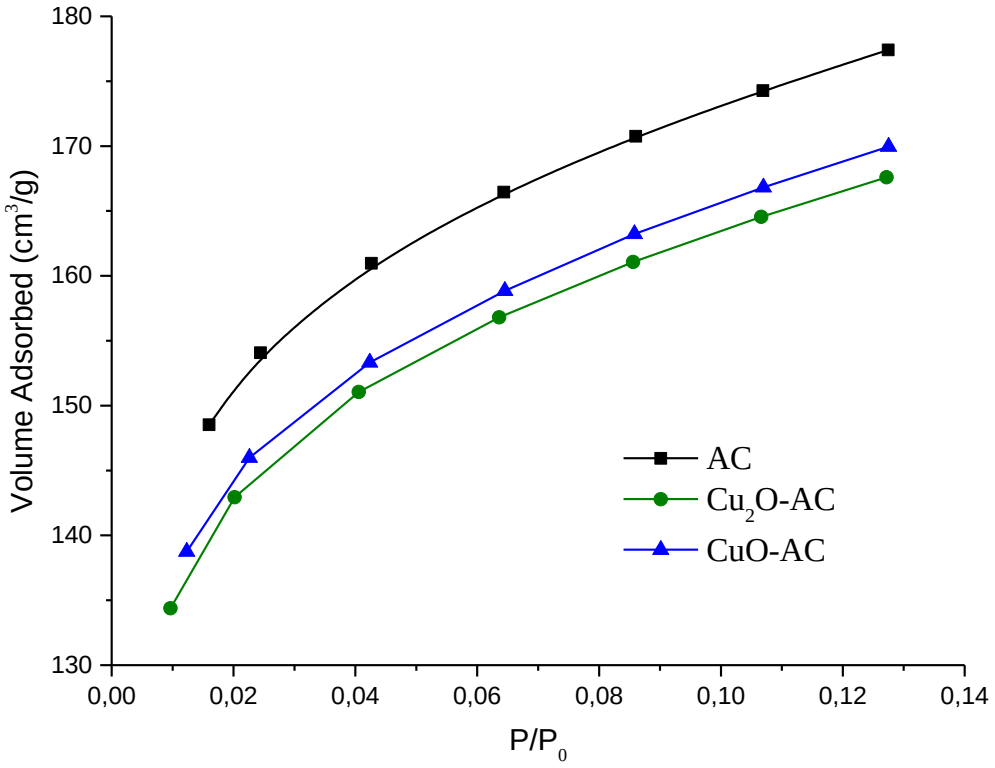

Figure 3.13. Nitrogen adsorption-desorption isotherms of activated carbon (AC) (square), Cu_2O nanoparticles loaded activated carbon (sphere) and CuO nanoparticles loaded activated carbon (triangle).

Table 3.1. Surface properties of activated carbon, activated carbon supported Cu_2O and CuO nanoparticles

	BET Surface area x 10^2 (m^2/g)	
Activated Carbon	6.809	
Cu_2O-Activated Carbon	6.526	
CuO-Activated Carbon	6.436	

Surface analyses by BET were performed to investigate surface area of activated carbon and copper oxide loaded activated carbon. A decrease in surface area of the activated carbon was observed in the presence of copper oxide nanoparticles as expected. (Table 3.1) The area has changed from 6.809 x 10^2 m^2/g to 6.526 x 10^2 and 6.436 x 10^2 m^2/g upon Cu_2O and CuO loading on activated carbon, respectively. No significant difference in surface area was observed between the CuO and Cu_2O nanoparticles loaded activated carbon. This observation suggests similar amount of coverage were achieved for both types of copper oxide nanoparticles on the support surface. Pore volume investigation was not performed for samples where activated carbon support used since it does not have well-defined porous structure.[58]

Figure 3.14 shows the nitrogen adsorption-desorption isotherms of zeolite and copper oxide nanoparticles on zeolite. Similar to activated carbon, Type I isotherm was observed for zeolite support, too. This verifies the microporous nature of the studied materials.[95]

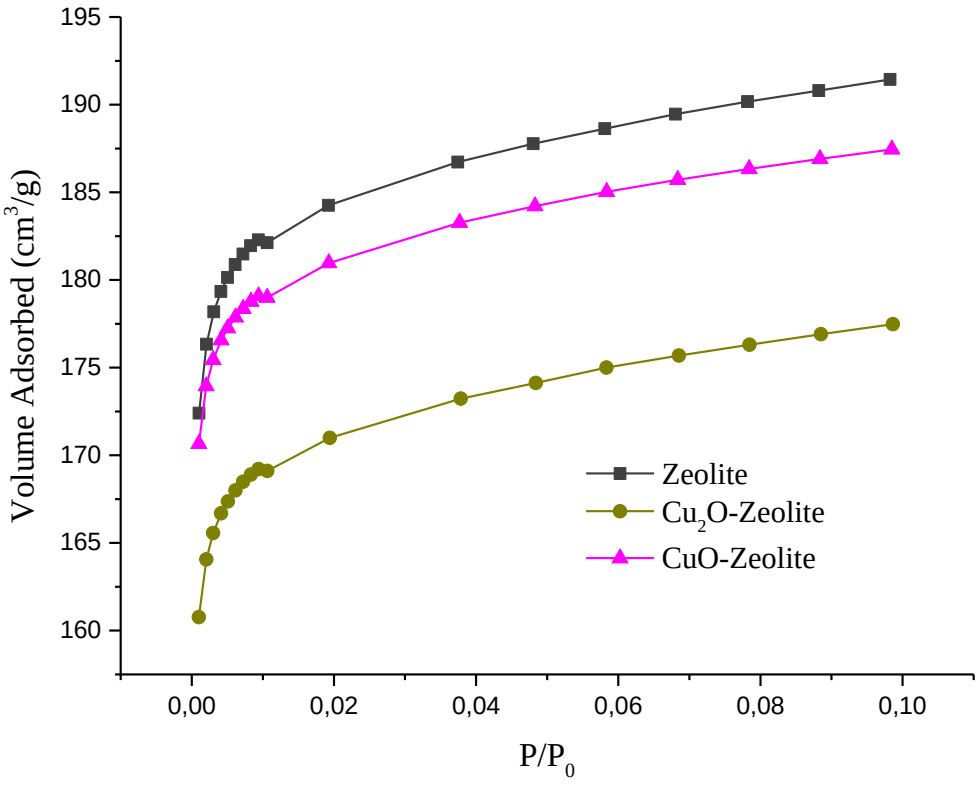

Figure 3.14. Nitrogen adsorption-desorption isotherms of zeolite (square), Cu_2O nanoparticles within zeolite (sphere), and CuO nanoparticles within zeolite (triangle).

Table 3.2. Surface properties of zeolite, zeolite supported Cu_2O and CuO nanoparticles

	BET Surface area (m^2/g)	Pore Volume (cm^3/g)
Zeolite	750	0.269
CuO-Zeolite	734	0.265
Cu_2O-Zeolite	695	0.249

The pore volume and area of zeolite and copper oxide nanoparticle loaded zeolite are given in Table 3.2. The decrease in surface area and micropore volume in copper oxide containing zeolite compared to the one of bare zeolite can be attributed to the encapsulation of copper oxide nanoparticles in zeolite framework. The surface area of zeolite decrease from 750 m^2/g to 734 and 695 m^2/g for CuO and Cu_2O nanoparticle containing zeolites, respectively. This decrease in zeolite surface area is resulted from copper oxide nanoparticle coating on both pore and exterior surface of the support. The pore volume of zeolite show slight decrease when CuO nanoparticles occupy its pores (from 0.269 to 0.265 cm^3/g). On the other hand, this decrease is more significant when Cu_2O exist in the pores (from 0.269 to 0.249 cm^3/g) indicating larger size of Cu_2O nanoparticles compared to the ones of CuO nanoparticles encapsulated in pores. This observation agrees well with the SEM and TEM analyses as discussed previously.

3.4. Investigating CO_2 Adsorption-Desorption Properties of Copper Oxide Nanoparticle Loaded Activated Carbon and Zeolite

CO_2 adsorption on surfaces can happen in two possible ways; physically and chemically. In physical adsorption, CO_2 and surface are interacting with weak intermolecular forces (i.e. van der Waals forces) and this interaction can be easily broken by thermal application at moderate temperatures. On the other hand, chemical adsorption (chemisorption) involves significantly stronger interaction, covalent bonding, between the CO_2 and adsorbent surface and much higher energy is needed to break this interaction.

CO_2 adsorption and desorption properties of copper oxide nanoparticles on two different support materials (activated carbon and zeolite) were thoroughly studied by taking physical and chemical adsorption of the gas molecules on both copper oxide nanoparticles as well as the ones on support materials. The details

of this investigation and discussion on findings are given in the following sections.

3.4.1. Quantitative measurement of CO_2 adsorption by TGA

The amounts of CO_2 adsorbed on copper oxide nanoparticle – active carbon/zeolite hybrid system were calculated by using TGA analysis. The way of CO_2 adsorption (physical/chemical) on both nanoparticles and supports were taken into consideration as the TGA data were examined.

It is important to emphasize the thermodynamic aspects of desorption of chemically adsorbed CO_2 from copper oxide surface before discussing TGA analysis results. As it was previously noted $CuCO_3$ formation occur as CO_2 chemically adsorb on copper oxide nanoparticle. The two possible routes for the decomposition of $CuCO_3$ and thermodynamic data associate with each route are summarized in Table 3.3. The temperatures given in the table represent the decomposition temperatures of $CuCO_3$ calculated by using the indicated ΔH, ΔS and ΔG values.[52] The thermodynamic data indicate the requirement of heat to break the strong interaction between O=C=O and copper oxide. The first route involves decomposition of $CuCO_3$ into CuO and CO_2 with a ΔH value of +45.5 kJ/mol^{-1} and can happen at temperatures as low as the room temperature.[48] In the second route, $CuCO_3$ decompose into Cu_2O, CO_2, and O_2. Enthalpy change (+233 kJ/mol^{-1}) associate with this reaction is much higher compared to the one of first route and the decomposition is spontaneous at higher temperatures (at 530 K or above). [48]

The experimental investigations show that higher temperatures are required for complete decomposition of $CuCO_3$ even though the release of CO_2 can possibly occur at much lower temperatures.[75] It has been reported that decomposition of $CuCO_3$ occur at temperatures of 583 K or above and thus the chemically

adsorbed CO_2 start to desorb at this temperature.[48] On the other hand, desorption of physically adsorbed CO_2 start to occur at lower temperatures (ca. 340 K).[48] Therefore, in this thesis study TGA analysis were performed at elevated temperatures up to 973 K to monitor the release of both physically and chemically adsorbed CO_2.

Table 3.3. Thermodynamics of reactions involving desorption of CO_2[48]

		ΔH *(kJ/mol^{-1})*	ΔS *(J.mol^{-1}/K^{-1})*	ΔG *(kJ/mol^{-1})*	T *(K)*
i)	$CuCO_{3(s)} \rightarrow CuO_{(s)} + CO_{2(g)}$	+45.5	+169	-4.9	298.0
ii)	$2CuCO_{3(s)} \rightarrow Cu_2O_{(s)} + 2CO_{2(g)} + 1/2O_{2(g)}$	+233.0	+447.6	-4.2	530.0

TGA curves for activated carbon, activated carbon with Cu_2O, and activated carbon with CuO after CO_2 adsorption are shown in Figure 3.15. The TGA curves demonstrate that the physically adsorbed CO_2 start to desorb at 343 K and the $CuCO_3$ (chemically adsorbed CO_2) start to decompose at 583 K. It is important to note that the observed decrease in mass is due to the CO_2 desorption from surfaces of both copper oxide nanoparticles and active carbon.

The amounts of physically and chemically adsorbed CO_2 by activated carbon and copper oxide nanoparticle decorated activated carbon calculated from this analysis in terms of percent weight loss, mass and volume of desorbed CO_2 are given in Table 3.4. The amounts of CO_2 physically adsorbed on activated carbon, Cu_2O and CuO nanoparticle loaded activated carbon are 0.091 mg, 0.059 mg and 0.253 mg, respectively. The decrease in the adsorbed amount on Cu_2O nanoparticle containing support compared to the bare support suggest that

physical adsorption of the CO_2 on these nanoparticles is not favorable. Therefore, existence of Cu_2O nanoparticles on active carbon surface resulted in a decrease in physically adsorbed CO_2 amount. On the other hand, the results indicate that physical adsorption on CuO nanoparticles is more favorable and the amount of physically adsorbed CO_2 increases with the existence of these nanoparticles on the support surface.

The comparison of the amounts of chemically adsorbed CO_2 on activated carbon (0.252 mg), Cu_2O and CuO nanoparticle containing active carbon (0.332 mg and 0.736 mg, respectively) show that chemisorption of CO_2 was increased with the presence of copper oxide nanoparticles on activated carbon. Similar to the physical adsorption results, here too, CuO nanoparticles increased the amount of chemically adsorbed CO_2 more compared to the Cu_2O nanoparticles. If both physical and chemical adsorptions of CO_2 are considered, the existence of Cu_2O and CuO nanoparticles on activated carbon surface increased the CO_2 adsorption capacity of activated carbon by 1.20 % and 13.1 %, respectively. The results suggest that CuO nanoparticles represent higher physical and chemical attractions towards CO_2 compared to Cu_2O nanoparticles. In other words, CuO nanoparticles are better sorbents than Cu_2O nanoparticles. The reason for high adsorption capacity of CuO nanoparticles can be considered as the high electronegativity of CuO compared to Cu_2O.[25] This increases the attraction between CuO and CO_2, thus CO_2 adsorption.

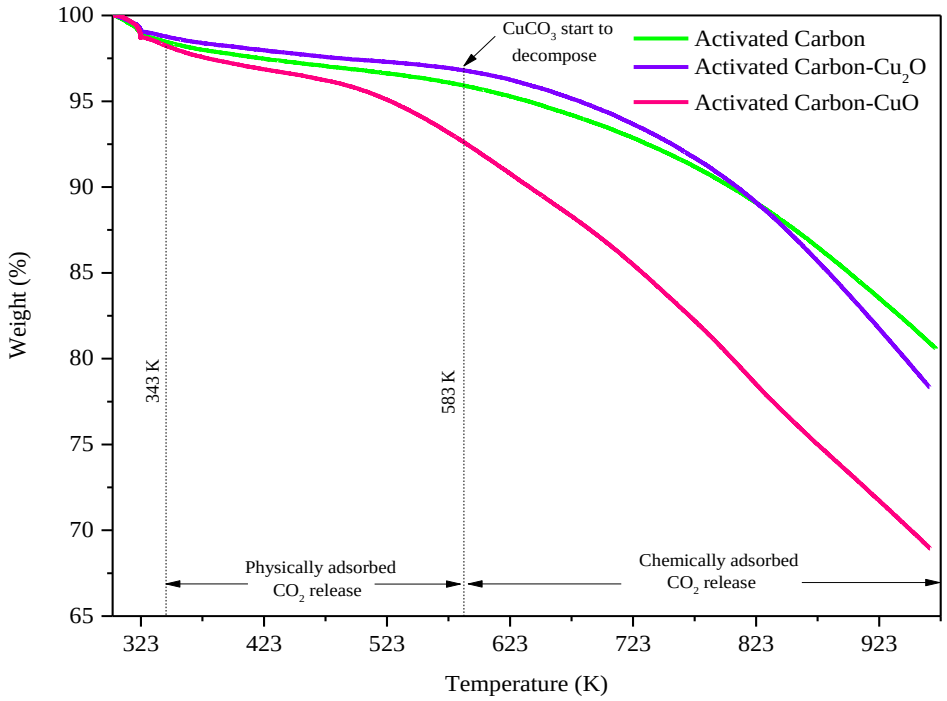

Figure 3.15. TGA curves for activated carbon (green line), activated carbon with Cu_2O nanoparticles (violet line), and activated carbon with CuO nanoparticles (pink line).

Table 3.4. The amount of CO_2 adsorbed by physically and chemically on activated carbon, activated carbon with Cu_2O, and activated carbon with CuO.

	Physically adsorbed CO_2			Chemically adsorbed CO_2		
	mg	%	cm^3	mg	%	cm^3
Activated Carbon	0.091	1.8	0.049	0.252	5.2	0.135
Activated Carbon-Cu_2O	0.059	1.2	0.032	0.332	7.1	0.178
Activated Carbon-CuO	0.253	4.9	0.135	0.736	15.2	0.394

*Density of CO_2 gas (1 atm 15 ^oC) is 1.87 kg/m^3. (This value was used for the calculation of volume of CO_2)

Figure 3.16 shows TGA curves for zeolite and copper oxide nanoparticle loaded zeolite after CO_2 adsorption. The region between 343 K and 583 K represent the temperature range where the complete desorption of physically adsorbed CO_2 from the surfaces occur. The slope change in the copper oxide-zeolite curve is observed at around 425 K. This is most likely the temperature where desorption of chemically adsorbed CO_2 starts. However, 583 K was used as a lower limit of chemically adsorbed CO_2 release in CO_2 amount calculations to make sure there is no contribution from physically adsorbed CO_2. As it was noted before, the amount of CO_2 released in this temperature range include the gas amounts physically adsorbed on both zeolite and copper oxide nanoparticles. Therefore, CO_2 desorption in the temperature range above 583 K represent the amount of the gas released from chemical adsorption which happens mainly on copper oxide nanoparticles.

Table 3.5 shows the amounts (in percent weight loss, mass and volume) of CO_2 physically and chemically adsorbed on zeolite and copper oxide loaded zeolites. The results show that physically adsorbed CO_2 amount increase when copper oxide nanoparticles (0.902 mg for Cu_2O and 0.903 mg for CuO) are loaded on the zeolite surfaces (0.792 mg). Similar trend is observed when the amounts of chemically adsorbed CO_2 are compared. As the 0.089 mg of CO_2 is adsorbed on zeolites, the amount is significantly increased to 0.168 mg and 0.224 mg upon Cu_2O and CuO nanoparticle loading, respectively. When total amounts of CO_2 (both physically and chemically adsorbed) on surfaces are compared, Cu_2O nanoparticle existence on zeolite increase the CO_2 adsorption 3.6 % as this amount increased 4.9 % with the CuO nanoparticle existence. These results reveal that CuO nanoparticles are better sorbents than the Cu_2O nanoparticles similar to the observation in activated carbon system. This is most likely due to higher electronegativity of CuO relative to Cu_2O nanoparticles, leading to stronger attraction for CO_2 toward CuO surfaces.[48]

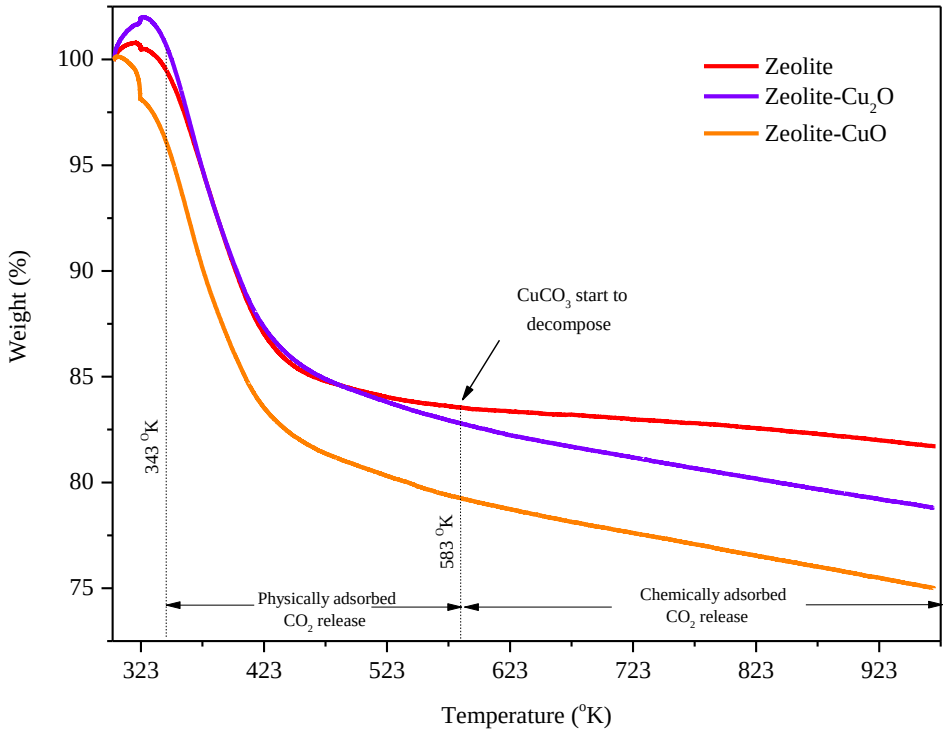

Figure 3.16. TGA curves for zeolite (red line), zeolite with Cu_2O nanoparticles (purple line), and zeolite with CuO nanoparticles (orange line).

Table 3.5. The amount of CO_2 adsorbed by physically and chemically on zeolite, zeolite with Cu_2O, and zeolite with CuO.

	Physically adsorbed CO_2			Chemically adsorbed CO_2		
	mg	%	cm^3	mg	%	cm^3
Zeolite	0.792	16.1	0.424	0.089	2.2	0.048
Zeolite-Cu_2O	0.902	17.8	0.482	0.168	4.0	0.090
Zeolite-CuO	0.903	17.8	0.483	0.224	5.3	0.120

*Density of CO_2 gas (1 atm 15 °C) is 1.87 kg/m^3. (This value was used for the calculation of volume of CO_2)

3.4.2. Qualitative and Quantitative measurements of CO_2 adsorption by FTIR

3.4.2.1. Qualitative measurements of CO_2 adsorption by FTIR

The FTIR spectra of bare supports (active carbon and zeolite), supports with Cu_2O nanoparticles, and supports with Cu_2O nanoparticles after CO_2 adsorption are given in Figure 3.17. The spectra given are single beam and not background corrected. The region below 2500 cm^{-1} in the spectra of all samples show absorption bands of CO_2 either in the air or on the surface.[18] The water bands adsorbed on surfaces or the ones of hydroxyl groups (i.e. $Cu(OH)_2$) are observed in the range between 3700 and 3100 cm^{-1} in the spectrum of all samples due to their interaction with air.[75]

Figure 3.17.a illustrates the spectra (4000-500 cm^{-1} range) of bare activated carbon, Cu_2O nanoparticles loaded on activated carbon, and Cu_2O nanoparticles loaded on activated carbon after CO_2 treatment. The peak at ~1730 cm^{-1} is assigned to C=C double bonds or C=O bonds in the structure of activated carbon.[103] The low signal level of the band is most likely due to use of small amount active carbon used for samples. Unfortunately, the IR light transmission through the active carbon is quite low. The light transmission through the sample decrease even further when Cu_2O nanoparticles are loaded on the surface of activated carbon. This result in further decrease in the signal intensity. The Figure 3.17.b shows the 1800-600 cm^{-1} region where the bands associated with the carbonate formed on Cu_2O nanoparticles- activated carbon system after CO_2 treatment are observed.[104] The observed bands are assigned as a combination band of bidentate carbonate or carboxylate at ~1570 cm^{-1} and monodentate carbonate at ~1520 cm^{-1}; monodentate carbonate band at ~815 cm^{-1}, sharp carboxylate bands at ~1388 cm^{-1}; bridge carbonate as shoulder at ~1265 cm^{-1}; broad bidentate carbonate bands at 886 cm^{-1} and 753 cm^{-1}.[75,105]

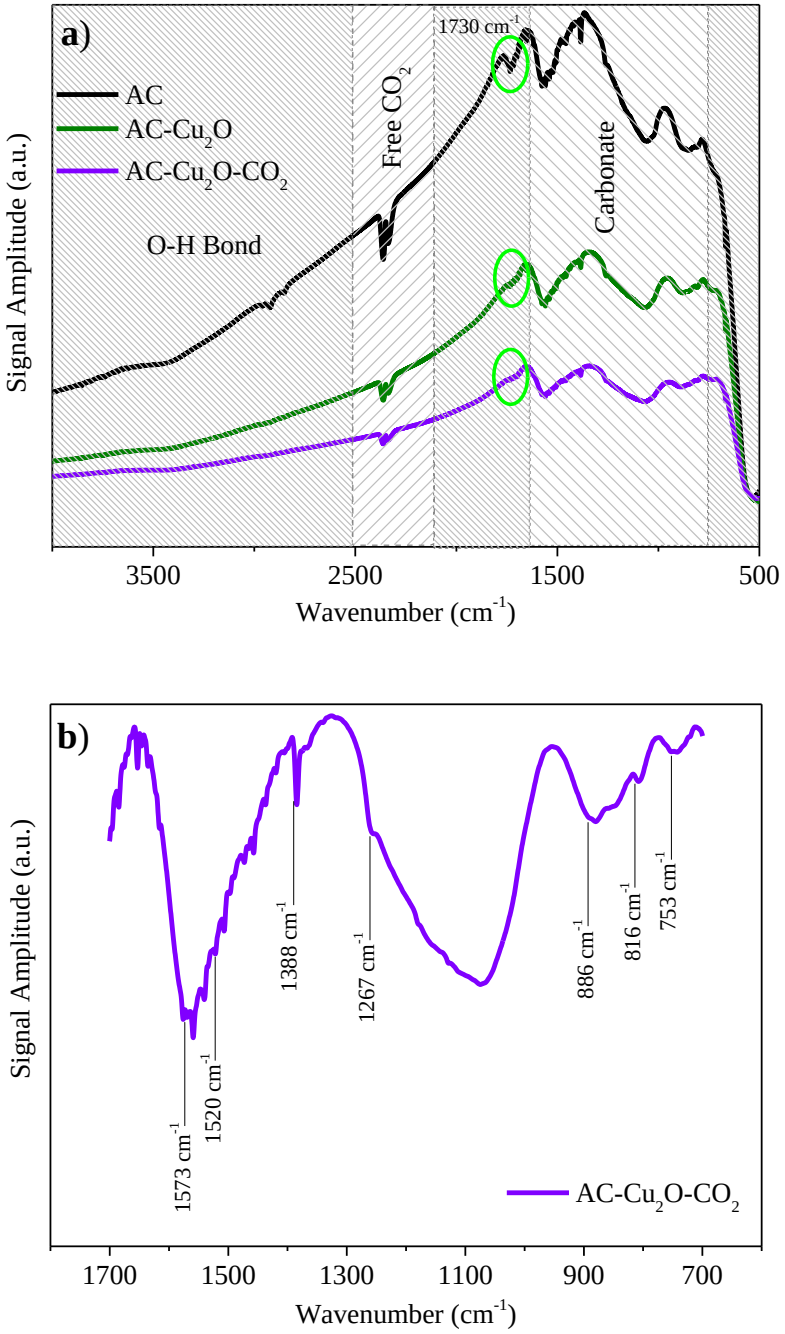

Figure 3.17. FTIR spectra of **a)** activated carbon (black dash), activated carbon with Cu_2O (olive dot), and activated carbon with Cu_2O after CO_2 adsorption (violet line), **b)** activated carbon with Cu_2O after CO_2 adsorption in the range between 1800-600 cm^{-1} (violet line)

Similarly, the FTIR spectra of zeolite, zeolite with Cu_2O nanoparticles, and Cu_2O nanoparticle loaded zeolite after CO_2 treatment are given in Figure 3.18.a. The zeolite samples have strong and broad features in 3700-3100 cm^{-1} region and 2260-1530 cm^{-1} region. These are mainly associated with the adsorbed water at the zeolite surface. As the broad and strong bands indicate, high amount of water adsorption is observed on zeolite surfaces due to their hydrophilic character. This strong water adsorption hinders the observation of the carbonate formation at the surface. The bands observed in 2500-2100 cm^{-1} region and 1525-1225 cm^{-1} region are of free CO_2 and carboxylate modes, respectively. A blow up of the 1525-1225 cm^{-1} region is given in Figure 3.18.b. The sharp band observed at 1384 cm^{-1} is of carboxylate mode[105] and shows the formation of carboxylate on Cu_2O nanoparticle surface. This mode is not observed in the spectrum of the bare zeolite.[84]

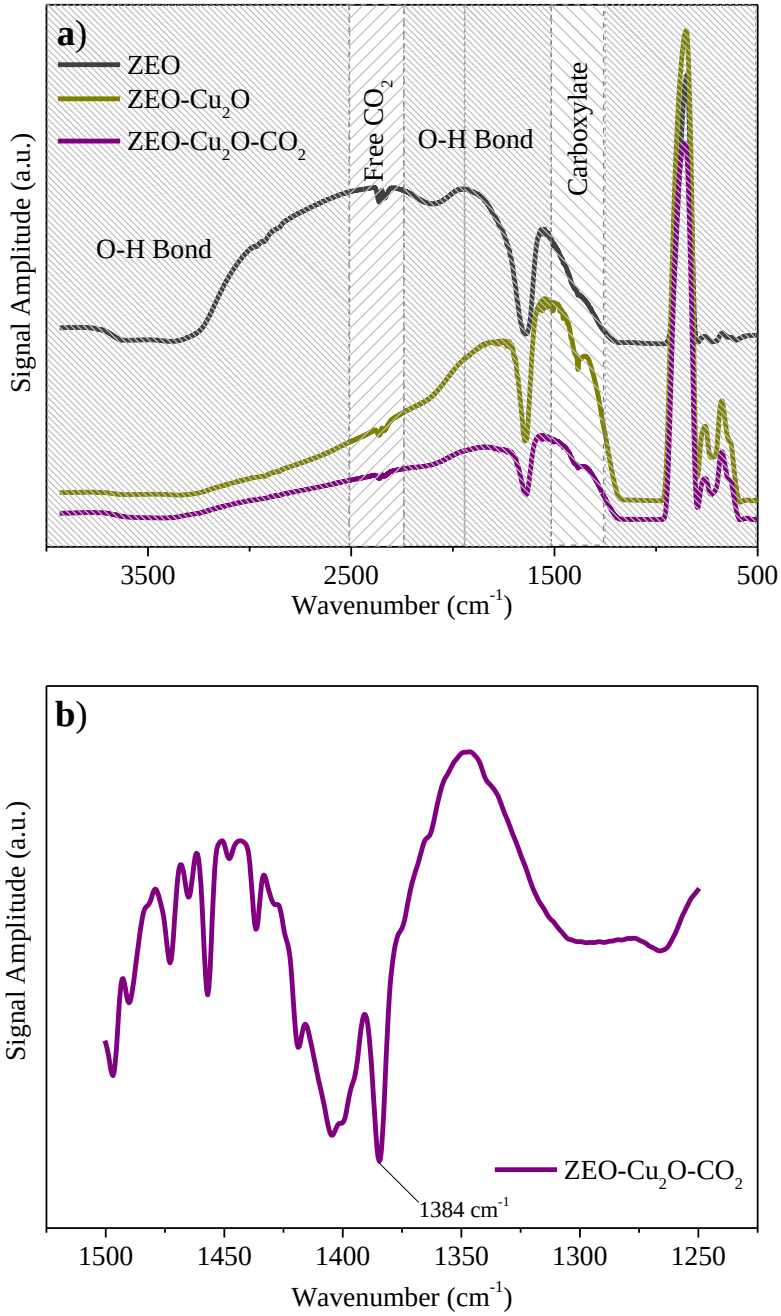

Figure 3.18. FTIR spectra of **a)** zeolite (gray dash), zeolite with Cu_2O (dark yellow dot), and zeolite with Cu_2O after CO_2 adsorption (purple line), **b)** zeolite with Cu_2O after CO_2 adsorption in the range between 1525-1225 cm^{-1} (purple line).

FTIR spectra of bare supports (active carbon and zeolite), supports with CuO, and supports with CuO after CO_2 treatment are given in Figure 3.19. The bands between 3700-3100 cm^{-1} for all samples shows that high amount of moisture or hydroxyl groups (in for $Cu(OH)_2$) are adsorbed on surfaces.[75] The spectra (4000-500 cm^{-1} range) of bare activated carbon, CuO nanoparticle loaded activated carbon, and CuO nanoparticle loaded activated carbon after CO_2 exposure are given in Figure 3.19.a. The bands in the range between 2500 and 2100 cm^{-1} shows the presence of free CO_2 on the surfaces..[18] The peak of aromatic rings, C=C bonds, or C=O bonds in the structure of activated carbon is located at ~1730 cm^{-1}.[103] The 1800-600 cm^{-1} range represent the carbonate region. Figure 3.19.b. shows the single beam spectra of the activated carbon with CuO nanoparticles after the CO_2 exposure. The observed bands are associated with the formation of the bidentate carbonate or carboxylate (at ~1573 cm^{-1}), monodentate carbonate (at ~1520 cm^{-1} and ~816 cm^{-1}), carboxylate (at ~1388 cm^{-1}), bridge carbonate (at ~1267 cm^{-1}), bidentate carbonate (at ~886 cm^{-1} and ~753 cm^{-1}).[75,105]

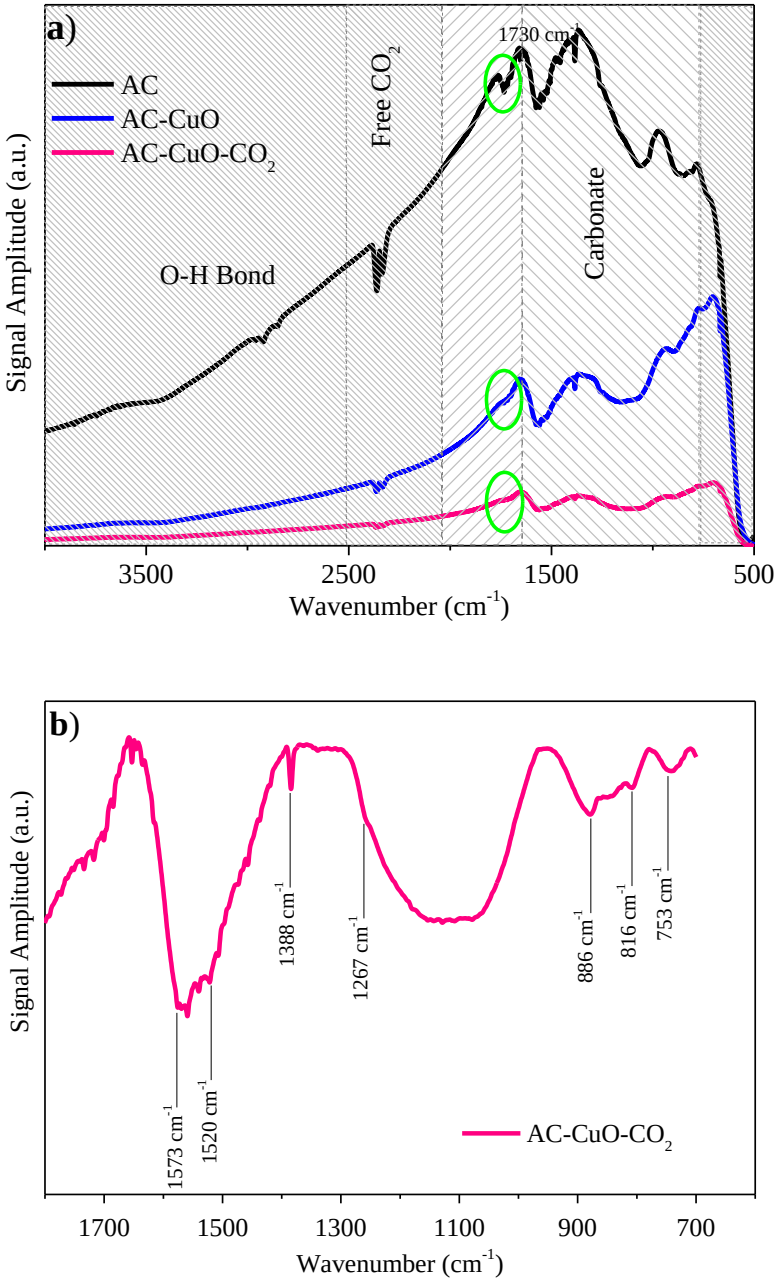

Figure 3.19. FTIR spectra of **a)** activated carbon (black dash), activated carbon with CuO (blue dot), and activated carbon with CuO after CO_2 adsorption (pink line), **b)** activated carbon with CuO after CO_2 adsorption (pink line) in the range between 1800-600 cm^{-1}

The FTIR spectra of zeolite, CuO nanoparticles-zeolite and CuO nanoparticles-zeolite systems after CO_2 adsorption are shown in Figure 3.20.a. Different from the activated carbon based systems, some moisture is observed on zeolite samples in 2260-1530 cm^{-1} region. This is due to the hydrophilic characteristic of zeolite as noted previously. A comparison of the zeolite only spectrum with the others shows that they are dominated by the zeolite features. The strong absorptions by the zeolite modes makes it difficult to identify the bands associated with the adsorbed CO_2, the carboxylate bands, especially around 1000 cm^{-1} where the zeolite absorbs the IR light very strongly. Figure 3.20.b shows the region (1525-1225 cm^{-1}) where the possible carbonate formation is observed. The sharp feature located at ~1384 cm^{-1} shows the presence of carboxylate ion at the surface after the CO_2 treatment. The rest of the carboxylate bands are hindered by strong water absorptions or strong zeolite absorptions.[105]

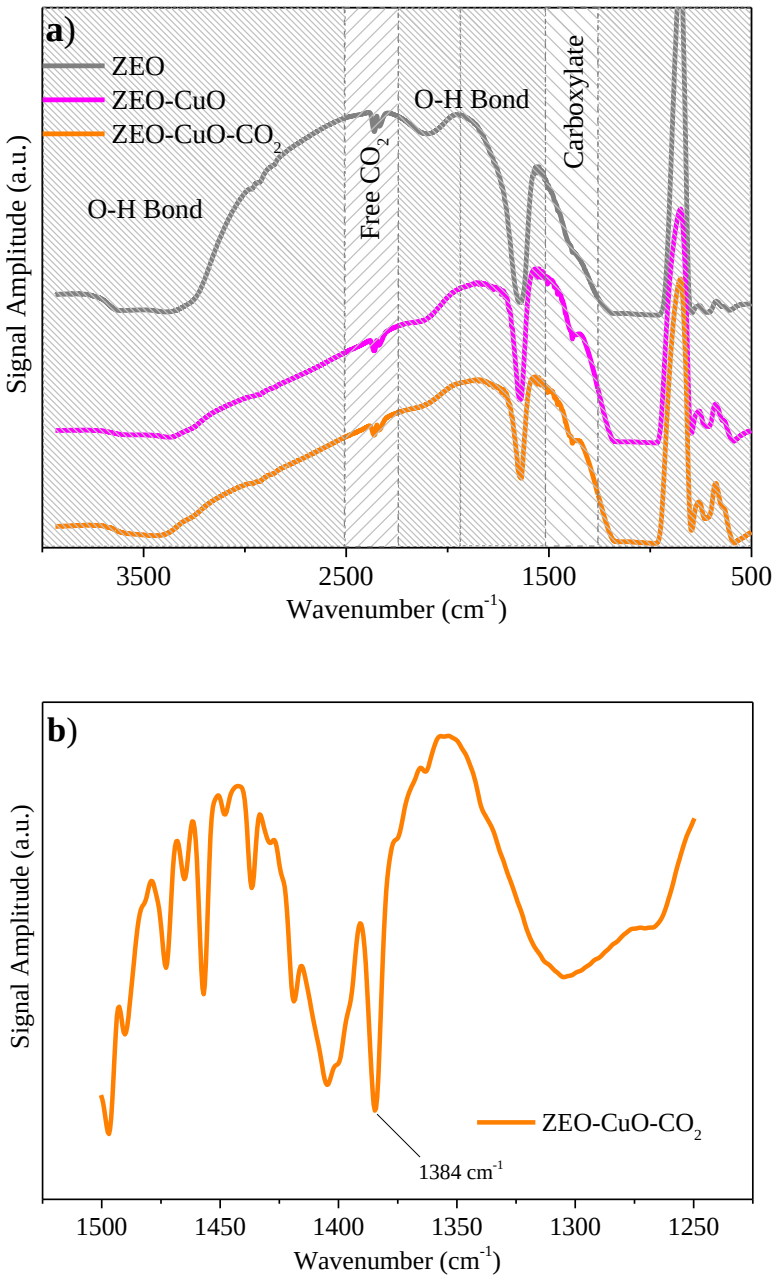

Figure 3.20. FTIR spectra of **a)** zeolite (gray dash), zeolite with CuO (magenta dot), and zeolite with CuO after CO_2 adsorption (orange line), **b)** zeolite with CuO after CO_2 adsorption in the range between 1525-1225 cm^{-1} (orange line)

The comparison of activated carbon and zeolite based systems reveal that zeolite adsorbs more water than activated carbon. This is because of the hydrophilic nature of the zeolite as the activated carbon is hydrophobic. On the other hand, the evaluation of FTIR spectra shows that the O-H band intensity decreases in the presence of copper oxide nanoparticles on supports suggesting decrease in the amount of adsorbed water on support surfaces. Thus, more active sites for CO_2 adsorption are created upon loading of copper oxide nanoparticles on support surface. Since it was not possible to determine the loaded Cu_2O or CuO amount either on active carbon support or on zeolite support, it was not possible to do neither a quantitative determination nor a relative amount of CO_2 adsorption on bare or decorated supports. A relative comparison of the adsorbed CO_2 on these samples via FTIR is going to be discussed in the next section.

3.4.2.2. Quantitative measurements of CO_2 adsorption by FTIR

A relative CO_2 adsorption capacity of supports, supports with Cu_2O nanoparticles, and supports with CuO nanoparticles were evaluated with the aid of FTIR analysis. The analysis was performed at room temperature by using a gas cell in ambient environment. The CO_2 gas mixture (5 % CO_2, 95 % N_2) was used as a reference.

The infrared light absorption of CO_2 in gas form is proportional to its concentration in the N_2:CO_2 gas mixture according to the Beer-Lambert Law[106]

$$A = \mathcal{E}.l.c$$

Here A is absorbance, $\mathcal{E}$ is absorptivity, l is the path length and c is the concentration of the CO_2. Thus, a ratio of two absorbance becomes a ratio of

the CO_2 concentrations in two different samples while the path length is kept constant:

$$A_1 / A_2 = c_1 / c_2,$$

Since concentration is proportional with the number of the CO_2 molecules:

$$c = (N/N_A)/V$$

The absorbance ratio directly becomes the ratio of the number of CO_2 molecules

$$A_1 / A_2 = N_1/N_2$$

Thus, the ratio directly shows the relative loss of the CO_2 in the sample compartment, which then can be correlated to the amount absorbed at the substrate surfaces when the reference N_2:CO_2 mixture is used. This enables ones to calculate the percentages of adsorbed CO_2 per gram of substrate for all samples.

The spectra of 5% CO_2 (as reference) and 5% CO_2 passed through the bare activated carbon, activated carbon with Cu_2O nanoparticles, and activated carbon with CuO nanoparticles adsorption were given in Figure 3.21. The observed spectrum of 5% CO_2 agree well with the one reported at the NIST database.[107] The strong CO_2 bending modes appear ca. 670 cm^{-1}. (Figure 3.21.a) Thus, it is more reliable to work in the range between 740 and 600 cm^{-1} than around the strong absorption band of CO_2.(Figure 3.21.b) A sharp decrease in the band associated with the CO_2 bending modes was observed when 5% CO_2 was passed through the samples. The evaluation of the data show that the existence of Cu_2O (olive line) and CuO (blue line) nanoparticles on activated carbon surface increased the adsorption capacity of

activated carbon (black line) by ~40 % and ~150 % per gram of the sample according to the absorption data as stated above when 5% CO_2 is taken as reference. The data also reveal that the activated carbon with CuO nanoparticles adsorbs much more CO_2 per gram of sample (~ 80%) than activated carbon with Cu_2O nanoparticles. These results are in good agreement with the ones observed in TGA analysis and verify that active carbon with CuO nanoparticles better sorbents than either bare active carbon or active carbon with Cu_2O nanoparticles.

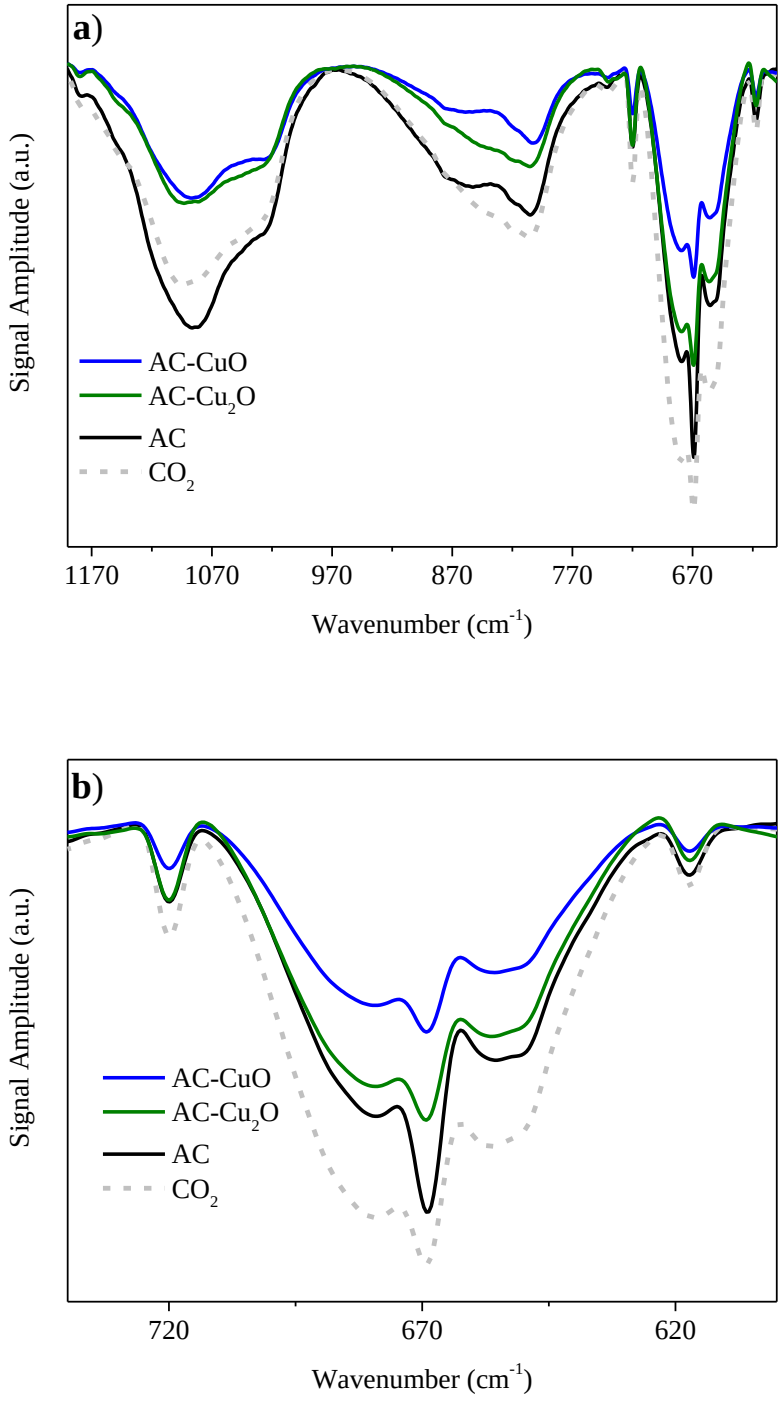

Figure 3.21. FTIR spectra of CO_2 (light gray dash line) and CO_2 passing after activated carbon adsorption (black line), activated carbon with Cu_2O adsorption (olive line), and activated carbon with CuO adsorption (blue line) in the ranges of **a)** 1200-600 cm^{-1} **b)** 600-800 cm^{-1}

The spectra of 5% CO_2 (as reference) and 5% CO_2 passed through the bare zeolite, zeolite with Cu_2O nanoparticles, and zeolite with CuO nanoparticles adsorption are given in Figure 3.22. Similar to the activated carbon based hybrid systems, here too, the spectrum (1200-600 cm^{-1} range) clearly shows CO_2 bands which agrees with the one reported in NIST database.[107] Similarly, the bands observed in 740-600 cm^{-1} region is used for reliable comparison. The analysis shows that presence of CuO and Cu_2O nanoparticles on zeolite increases the CO_2 adsorption by ca. 155% and ca. 30 %, respectively. The comparison of these two nanoparticle systems verifies significantly higher CO_2 capture capability of CuO nanoparticles (ca. 90% / g) compared to the one of Cu_2O nanoparticles similar to the observations in previous active carbon systems.

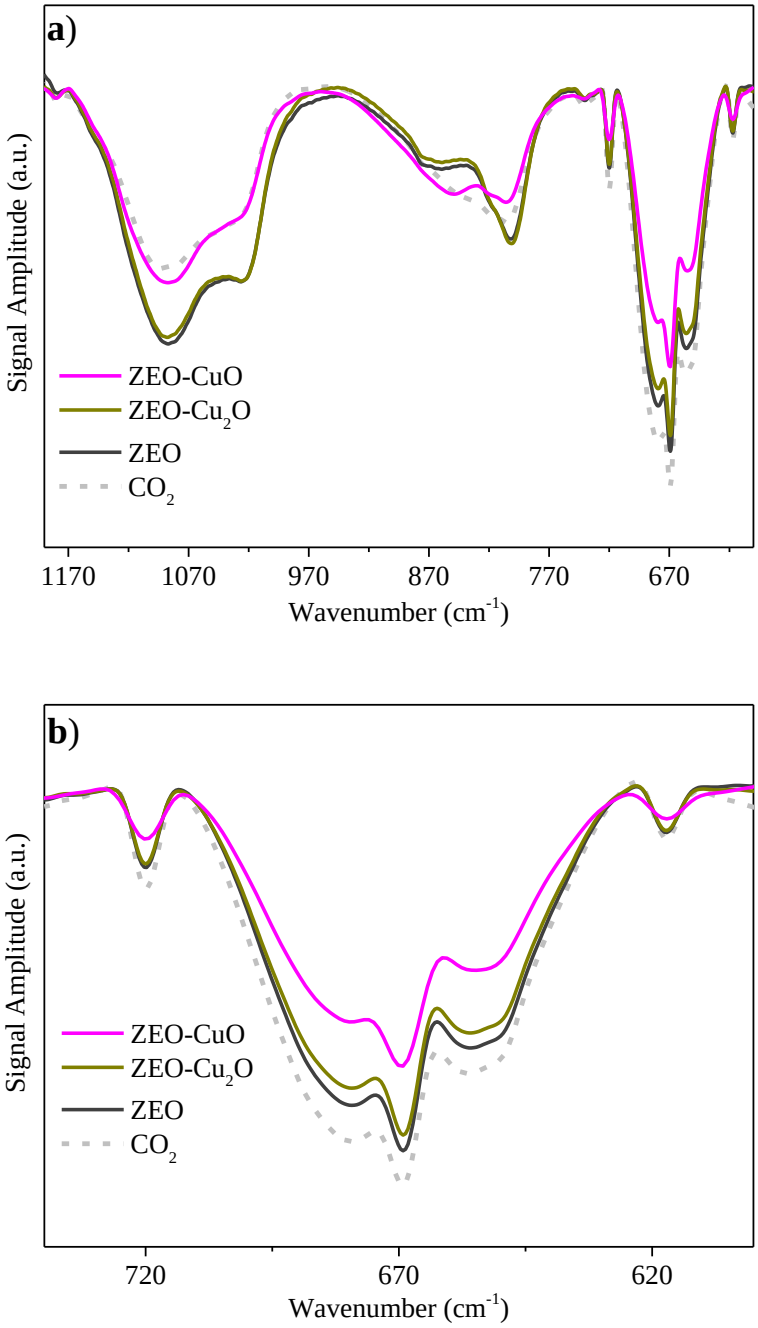

Figure 3.22. FTIR spectra of CO_2 (light gray dash line) and CO_2 passing after zeolite adsorption (dark gray line line), zeolite with Cu_2O adsorption (dark yellow line), and zeolite with CuO adsorption (magenta line) in the ranges of **a)** 1200-600 cm^{-1} **b)** 600-800 cm^{-1}.

3.4.3. Analysis of carbonate formation by XPS

XPS analysis was performed to complement the results obtained from FTIR analysis for observing carbonate formation after chemical adsorption of CO_2 on copper oxide nanoparticle - support hybrid system. Even though this analysis was performed for all copper oxide – support (activated carbon, zeolite) systems, only the CuO nanoparticle loaded zeolite yielded detectable copper signals allowing the evaluation of results. This observation was expected since the weak signals of copper were observed in the XPS analysis of CuO nanoparticles on activated carbon and Cu_2O nanoparticles on both zeolite and activated carbon as discussed in previous sections. Therefore, the analysis results obtained from only CuO-zeolite system are discussed in this section and the XPS spectra of others are given in appendix Figure A.4.

XPS spectra of CuO nanoparticle loaded zeolite after CO_2 adsorption are given in Figure 3.23. The spectrum for C1s shows two peaks at 283.4 eV and 288.0 eV (Figure 3.23.a) The one at 283.4 eV correspond to C_α where the reference value is 284.5.[75] The peak at 288.0 eV was assigned to carbonate based on the reported literature value (289.0 eV).[75]

The O1s spectrum demonstrates two peaks at 530.7 eV and 529.2 eV with a difference of 1.5 eV. (Figure 3.23.b) These values are in very good agreement with the previously reported ones which are 530.6 eV and 532.1 eV (1.5 eV difference) for CuO and $CuCO_3$, respectively.[75] Therefore, the XPS spectrum of O1s suggests the presence of both CuO and $CuCO_3$ in the sample of zeolite with CuO after 2 hours of CO_2 exposure. Furthermore, it is important to note that SiO_2 (532.9 eV), Al_2O_3 (531.2 eV), and Na_2O (529.6 eV) present in zeolite framework structure and they are expected to make contributions to the observed O1s peak located at 530.7 eV.[108] This is considered as the most likely reason for significantly high intensity of the O1s peak at 283.4 eV.

The Cu 2p core level XPS spectrum is given in Figure 3.23.c. The spectrum shows two Cu2p peaks with binding energies of 933.5 eV and 931.9 eV. The difference in these peaks was calculated as 1.6 eV. The position of the peaks and difference between them agree well with the CuO (933.0 eV) and $CuCO_3$ (934.8 eV) peaks reported for CuO powders after CO_2 adsorption.[75] This suggests that $CuCO_3$ formation occurs after exposing CuO nanoparticles to CO_2. Strong satellites peaks indicating the presence of CuO nanoparticles which did not capture CO_2 in the medium were observed.[101,102] This. These results demonstrate significant amount of CO_2 has been chemically adsorbed by CuO nanoparticles on zeolite surface suggesting them to be good sorbents for capturing CO_2 at room temperature.

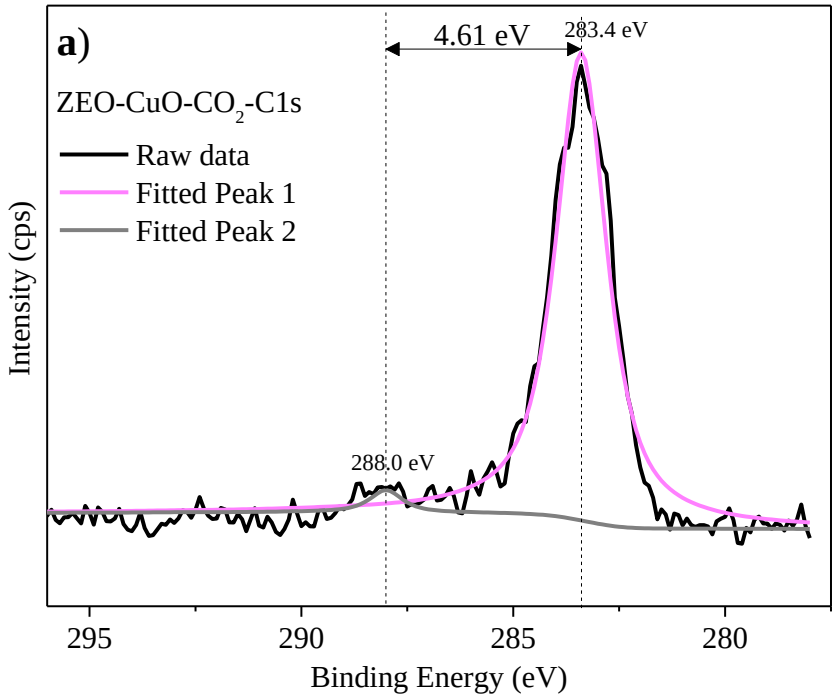

Figure 3.23. XPS spectra of zeolite with CuO after adsorption of CO_2, **a)** C 1s, **b)** O 1s, **c)** Cu 2p

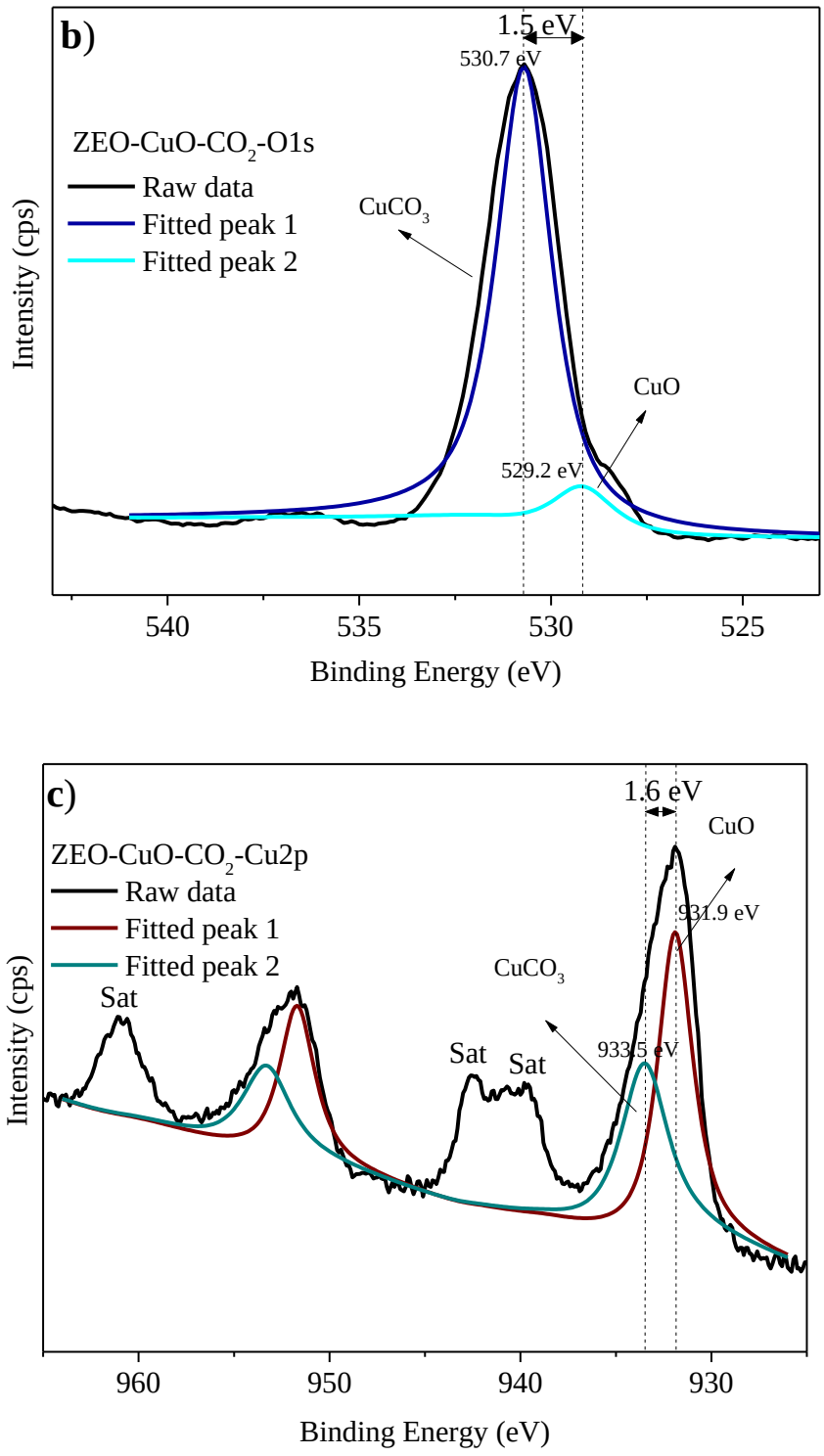

Figure 3.23. XPS spectra of zeolite with CuO after adsorption of CO_2, **a)** C 1s, **b)** O 1s, **c)** Cu 2p (continued)

CHAPTER 4

CONCLUSIONS

CO_2 emission is becoming a global concern for the entire world due to its contribution to global warming. Developing new carbon dioxide capture and storage technologies has attracted a great attention as they provide storing CO_2 for its further use in several applications such as production of carbonated beverages, transporting and preserving tissues, treatment of waste water etc. In this technology, supports such as zeolite and activated carbon are considered as great hosts for keeping gas molecules. Implanting copper oxide nanoparticles on the surface of these materials is suggested to improve *i)* the CO_2 adsorption due to the increase in the overall surface area, and *ii)* the gas storage because of the formation of stronger interaction (chemical adsorption) between the gas molecule and the copper oxide nanoparticles.

In this study, syntheses of CuO and Cu_2O nanoparticles on activated carbon and zeolite surface were achieved by precipitation method. Then the CO_2 adsorption capacities of copper oxide loaded supports (activated carbon and zeolite) were investigated.

Characterization of morphologies and chemical identities of copper oxide nanoparticles on supports were done by TEM, SEM, EDX, XRD and XPS analyses. SEM and TEM analyses show that the Cu_2O nanoparticles form in spherical-like shape on supports (zeolite and activated carbon) with the average size of 45±5 nm. On the other hand, CuO nanoparticles have sharper features with avarage size of 60±5 nm. The images also show that Cu_2O nanoparticles on both support and CuO ones on activated carbon are well dispersed on support

surface, but CuO nanoparticles seem to form assemblies growing out of the surface.

Existence of copper oxide nanoparticles and their type (Cu_2O or CuO) on support surfaces were investigated via XRD and XPS analysis. In XRD analysis, most of the Cu_2O or CuO peaks could not be clearly observed due to the significantly lower amount of these nanoparticles on support surface compared to the amount of support material. On the other hand, some of obsevable signature peaks of the copper oxide nanoparticles allowed us to identify Cu_2O nanoparticles on zeolite, CuO on activated carbon and zeolite. Similarly, in XPS analysis too, clear identification of nanoparticles has been hampered by their low loading on exterior surface of support. This analysis also verified the existance of copper oxide nanoparticles on support surface. However, only CuO nanoparticles on zeolite surface has been clearly identified by this technique. This is mostly because of the existence of significant amount of CuO nanoparticle assemblies on exterior surface of zeolite.

CO_2 adsorption capabilities and surface characteristics of copper oxide nanoparticles on support of interest have been investigated by BET, TGA, FTIR, and XPS Analysis. Copper oxide loaded supports exhibited type I isotherm that belongs to mesoporous materials according to nitrogen adsorption-desorption isotherms. BET analysis showed that surface area of supports decreased after loading of copper oxide nanoparticles as expected. It suggests the formation of copper oxide nanoparticles interior and exterior surfaces. Pore volume analysis for zeolite supported Cu_2O and CuO nanoparticles demonstrated a significant decrease in pore volume of the support upon nanoparticle loading. Moreover, comparison of the decrease amount in pore volume verified the larger size of Cu_2O nanoparticles relative to CuO ones.

In TGA analysis, the amounts of CO_2 adsorption of copper oxide nanoparticles loaded supports were calculated. The amount of adsorbed CO_2 (both physically

and chemically) has increased by 1.204 % and 13.05 % in presence of Cu_2O and CuO nanoparticles on activated carbon surface, respectively. Similarly, increase in the CO_2 adsorption amount has also observed on zeolite supported nanoparticles. The amount of adsorbed CO_2 has increased by 3.613 % and 4.875 % upon loading of Cu_2O and CuO nanoparticles on zeolite surface, respectively. These analyses suggest that presence of copper oxide nanoparticles increase the CO_2 adsorption capacity of supports and between two types of copper oxide nanoparticles, CuO one is better sorbent than the Cu_2O nanoparticles.

In FTIR analysis, qualitative and quantitative analysis of adsorbed CO_2 was performed. The strong absorption bands were monitored between the ranges 1800 and 600 cm^{-1} corresponded to carbonate formation on activated carbon samples after CO_2 treatment. However, the only peak located at 1384 cm^{-1} referring to carboxylate was observed on zeolite sample after CO_2 treatment because of the suppression of peaks belonging to zeolite structure. According to FTIR spectra of CO_2 between 740 and 600 cm^{-1}, presence of Cu_2O nanoparticles and CuO nanoparticles on activated carbon surface increased the adsorption capacity of bare activated carbon by 38% and 153% per gram, respectively. The spectra also show that CuO nanoparticles adsorbed more CO_2 (83% per gram) than Cu_2O nanoparticles. Similar trend was observed in Cu_2O zeolite samples. The presence of Cu_2O nanoparticles within zeolite and CuO nanoparticles within zeolite increased the amount of adsorbed CO_2 by bare zeolite by 33% and 155% per gram. Furthermore, CuO nanoparticles much better sorbent than Cu_2O nanoparticles. It adsorbed more CO_2 (92% per gram of sample) than Cu_2O nanoparticles.

XPS analyses results also complement the ones observed from TGA and FTIR studies. Even though the copper carbonate formation could only be clearly detected on CuO nanoparticle loaded zeolite system, the analysis verified the presence of copper oxide nanoparticles on all studied support surfaces

In conclusion, the adsorption capacity of zeolite and activated carbon supports has been improved by loading of copper oxide nanoparticles on their surface. Moreover, the developed hybrid system has provided stronger adsorption of CO_2 via chemical bond on the copper oxide nanoparticles compared to its relatively weak adsorption on supports (zeolite and active carbon). This makes the copper oxide loaded support hybrid system very promising for not only CO_2 adsorption but also trapping and storing the gas for its further use in industry. The results obtained from this study are believed to contribute to the developments in the CO_2 capturing and storage technology.

REFERENCES

(1) Zahmakiran, M.; Özkar, S. *Mater. Lett.* **2009**, *63* (12), 1033–1036.

(2) Vijaikumar, S.; Subramanian, T.; Pitchumani, K. *J. Nanomater.* **2008**, *2008* (1).

(3) Othman Ali, I. *Mater. Sci. Eng. A* **2007**, *459* (1-2), 294–302.

(4) Pohl, M.; Otto, a. *Surf. Sci.* **1998**, *406* (1-3), 125–137.

(5) Mondal, M. K.; Balsora, H. K.; Varshney, P. *Energy* **2012**, *46* (1), 431–441.

(6) Kaithwas, A.; Prasad, M.; Kulshreshtha, A.; Verma, S. *Chem. Eng. Res. Des.* **2012**, *90* (10), 1632–1641.

(7) EPA. U.S. Environmental Protection Agency: Washington, DC, USA.

(8) U.S. Department of State. Washington, DC, USA, 2007.

(9) IPCC. In *based on global emissions from 2010, the contribution of Working Group III to the Fifth Assessment Report of the Intergovernmental Panel on Climate Change.*; 2014.

(10) Stephen A. Rackley. *Carbon Capture and Storage*; Elsevier: USA, 2010.

(11) Olajire, A. a. *Energy* **2010**, *35* (6), 2610–2628.

(12) Li, B.; Duan, Y.; Luebke, D.; Morreale, B. *Appl. Energy* **2013**, *102*, 1439–1447.

(13) National Research Council. Washington, DC, USA, 2010.

(14) Seul-yi, Q.; Park, S. *J. Ind. Eng. Chem.* **2014**.

(15) OECD. In *The OECD Environmental Outlook Baseline projections*; 2014.

(16) Keeling, C.D., Whorf, T. P. *Oak Ridge Natl. Lab.* **1998**.

(17) Metz, B., Davidson, H., Meyer, L., Loos, M., C. H. *IPCC Special Report Carbon Dioxide Capture and Storage*; New York, 2014.

(18) Dantas, T. L. P.; Luna, F. M. T.; Silva, I. J.; de Azevedo, D. C. S.; Grande, C. a.; Rodrigues, A. E.; Moreira, R. F. P. M. *Chem. Eng. J.* **2011**, *169* (1-3), 11–19.

(19) Marszałek, K.; Skąpska, S.; Woźniak, Ł.; Sokołowska, B. *Innov. Food Sci. Emerg. Technol.* **2015**, *32*, 101–109.

(20) Aresta, M.; Eugenio, Q.; Immacolata, T. *Report* **2004**, 1341–1344.

(21) Liu, Z. *Appl. Energy* **2015**.

(22) Arenillas, A., Smith, K.M., Drage, T.C., Snape, C. E. *Fuel 84, 2204-2210* **2005**.

(23) Lee, S. J., Park, J. *Ind. Eng. Chem.* **2014**.

(24) Adams, D., Davidson, J. *IEA Greenh. Gas R&D Progr.* **2007**, *ISBN 978-1*, 17.

(25) Yin, C.; Yan, J. *Appl. Energy* **2016**, *162*, 742–762.

(26) Wilcox; Babcock. *Steam: Its Generation and Use*, 40 th.; The Babcocks and Wilcox Company: Barberton,Ohio, 1992.

(27) Figueroa, J. D., Fout, T., Plasynski, S., McIlvried, H., Srivastava, R. D. *Int. J. Greenh. Gas Control* **2008**, 9–20.

(28) Damen, K., Troost, M.V., Faaij, A., Turkenburg, W. *Prog. Energy Combust. Sci.* **2006**, 215–246.

(29) Blomen, E., Hendriksa, C., Neele, F. *Energy Procedia* **2009**, 1505–1512.

(30) Kim, Y.E., Moon, Y.I., Yoon, Y.I., Jeong S.K., Park, K.T., Bae, S.T., Nam, S. C. *Sep. Purif. Technol. 122 (2014).*

(31) Sistla, Y. S.; Khanna, A. *J. Ind. Eng. Chem.* **2013**, *20* (4), 2497–2509.

(32) Lee, A. S.; Eslick, J. C.; Miller, D. C.; Kitchin, J. R. *Int. J. Greenh. Gas Control* **2013**, *18*, 68–74.

(33) Kenarsari, S.D., Yang, D., Jiang, G., Zhang, S., Wang, J., Russell, A.G., Wei, Q., Fan, M. *RSC Adv.* **2013**, *3*, 22739.

(34) Zhang, X., He, X., Gundersen, T. *Energy Fuels* **2013**, *27*, 4137.

(35) Zhao, C.; Chen, X.; Zhao, C.; Wu, Y.; Dong, W. *Energy & Fuels* **2012**, *26* (5), 3062–3068.

(36) Kim, K.; Son, Y.; Lee, W. B.; Lee, K. S. *Int. J. Greenh. Gas Control* **2013**, *17*, 13–24.

(37) Roth, E.A., Agarwal, S., Gupta, R. K. *Energy Fuels* **2013**, *27*, 4129.

(38) Scholes, C. a.; Ho, M. T.; Wiley, D. E.; Stevens, G. W.; Kentish, S. E. *Int. J. Greenh. Gas Control* **2013**, *17*, 341–348.

(39) Song, C. F.; Kitamura, Y.; Li, S. H. *Appl. Energy* **2012**, *98*, 491–501.

(40) Choi, W. J.; Seo, J. B.; Jang, S. Y.; Jung, J. H.; Oh, K. J. *J. Environ. Sci.* **2009**, *21* (7), 907–913.

(41) Figueroa, J. D.; Fout, T.; Plasynski, S.; McIlvried, H.; Srivastava, R. D. *Int. J. Greenh. Gas Control* **2008**, *2* (1), 9–20.

(42) Gibbins, J.; Chalmers, H. *Energy Policy* **2008**, *36* (12), 4317–4322.

(43) Damen, K.; Troost, M. Van; Faaij, A.; Turkenburg, W. *Prog. Energy Combust. Sci.* **2006**, *32* (2), 215–246.

(44) Spigarelli, B. P.; Kawatra, S. K. *J. CO_2 Util.* **2013**, *1*, 69–87.

(45) Khoo, H. H.; Tan, R. B. H. *Environ. Sci. Technol.* **2006**, *40* (12), 4016–4024.

(46) AxeL, M., Xiaoshan, S. *Energy Convers. Manag.* **1997**, *38*, 37–42.

(47) Ma'mun, S.; Svendsen, H. F.; Hoff, K. a.; Juliussen, O. *Energy Convers. Manag.* **2007**, *48* (1), 251–258.

(48) Yong, Z.; Mata, V.; Rodrigues, E. **2002**, *26*, 195–205.

(49) Son, W.-J.; Choi, J.-S.; Ahn, W.-S. *Microporous Mesoporous Mater.* **2008**, *113* (1-3), 31–40.

(50) Balsamo, M.; Rodríguez-Reinoso, F.; Montagnaro, F.; Lancia, A.; Erto, A. *Ind. Eng. Chem. Res.* **2013**, *52* (34), 12183–12191.

(51) Balsamo, M.; Budinova, T.; Erto, a.; Lancia, a.; Petrova, B.; Petrov, N.; Tsyntsarski, B. *Sep. Purif. Technol.* **2013**, *116*, 214–221.

(52) Shafeeyan, M. S.; Mohd, W.; Wan, A.; Houshmand, A.; Shamiri, A. *J. Anal. Appl. Pyrolysis* **2010**, *89* (2), 143–151.

(53) Marsh, H., Rodriguez-Reinoso, F. *Activated Carbon*, 1st ed.; Elsevier Ltd: USA, 2006.

(54) Marsh, H., Rodriguez-Reinoso, F. *Activated Carbon*, 1st ed.; Elsevier Ltd.: USA, 2006.

(55) Arenillas, a.; Rubiera, F.; Parra, J. B.; Ania, C. O.; Pis, J. J. *Appl. Surf. Sci.* **2005**, *252* (3), 619–624.

(56) Drage, T. C.; Arenillas, a.; Smith, K. M.; Pevida, C.; Piippo, S.; Snape, C. E. *Fuel* **2007**, *86* (1-2), 22–31.

(57) Kwiatkowski, J. F. *Activated Carbon; Classification, properties, and applications*, 1st ed.; Chemical Engineerin Methods and Technology, 2011.

(58) Saxena, R.; Singh, V. K.; Kumar, E. A. *Energy Procedia* **2014**, *54*, 320–329.

(59) Caglayan, B. S., Aksoylu, A. E. *J. Hazard. Mater.* **2013**, *252-253*, 19–28.

(60) Alabadi, A., Razzaque, S., Yang, Y., Chen, S., Tan, B. *Chem. Eng. J.* **2015**, *281*, 606–612.

(61) Barton, T. J., Bull, L. M., Klemperer, W. G., Loy, D. A., McEnaney, B., Misono, M., Monson, P. A., Pez, G., Schere, G. W., Vartuli, J. C., Yaghi, O. M. *Chem. Mater.* **1999**, *11* (10), 2633–2656.

(62) Auerbach, S. M., Carrado, K. A., Dutta, P. K. *Handbook of Zeolite Science and Technology*, 1st ed.; Marcel Dekker: USA, 2003.

(63) Walton, K. S.; Abney, M. B.; LeVan, M. D. *Microporous Mesoporous Mater.* **2006**, *91* (1-3), 78–84.

(64) Zhang, J.; Singh, R.; Webley, P. a. *Microporous Mesoporous Mater.* **2008**, *111* (1-3), 478–487.

(65) He, P.; Wang, W.; Du, L.; Dong, F.; Deng, Y.; Zhang, T. *Anal. Chim. Acta* **2012**, *739*, 25–30.

(66) Chen, C.; Park, D.-W.; Ahn, W.-S. *Appl. Surf. Sci.* **2014**, *292* (FEBRUARY), 63–67.

(67) P., E. P. *J. Am. Chem. Soc.* **1995**, *117* (1), 9087.

(68) Kaduk, J. a; Faber, J. *Rigaku J.* **1995**, *12* (2), 14–34.

(69) Smykowski, D.; Szyja, B.; Szczygiel, J. *J Mol Graph Model* **2014**, *50*, 35–43.

(70) Hudson, M. R.; Queen, W. L.; Mason, J. a.; Fickel, D. W.; Lobo, R. F.; Brown, C. M. *J. Am. Chem. Soc.* **2012**, *134* (4), 1970–1973.

(71) Freund, H. J., Roberts, M. W. *Surf. Sci. Rep.* **1996**, *25*, 227.

(72) Selen, B.; Aksoylu, A. E. *J. Hazard. Mater.* **2013**, *252-253*, 19–28.

(73) Abee, M. W.; York, S. C.; Cox, D. F. **2001**, *3* (0001), 7755–7761.

(74) Jeon, H., Min, Y. J., Ahn, S. H., Hong, S. M., Shin, J. S., Kim, J. H., Lee, K. B. *Colloids Surfaces A Physicochem. Eng. Asp.* **2012**, *414*, 75–81.

(75) Isahak, W. N. R. W.; Ramli, Z. A. C.; Ismail, M. W.; Ismail, K.; Yusop, R. M.; Hisham, M. W. M.; Yarmo, M. A. *J. CO_2 Util.* **2013**, *2*, 8–15.

(76) Jang, D. I., Park, S. J. *Fuel* **2012**, *102*, 439–444.

(77) Kim, B. J.; Cho, K. S.; Park, S. J. *J. Colloid Interface Sci.* **2010**, *342* (2), 575–578.

(78) Nath, D.; Banerjee, P. *Environ. Toxicol. Pharmacol.* **2013**, *36* (3), 997–1014.

(79) Baltrusaitis, J.; Schuttlefield, J.; Zeitler, E.; Grassian, V. H. *Chem. Eng. J.* **2011**, *170* (2-3), 471–481.

(80) Jeon, H.; Min, Y. J.; Ahn, S. H.; Hong, S.-M.; Shin, J.-S.; Kim, J. H.; Lee, K. B. *Colloids Surfaces A Physicochem. Eng. Asp.* **2012**, *414*, 75–81.

(81) López-Bastidas, C.; Petranovskii, V.; Machorro, R. *J. Colloid Interface Sci.* **2012**, *375* (1), 60–64.

(82) El-Trass, a.; Elshamy, H.; El-Mehasseb, I.; El-Kemary, M. *Appl. Surf. Sci.* **2012**, *258* (7), 2997–3001.

(83) Phiwdang, K.; Suphankij, S.; Mekprasart, W.; Pecharapa, W. *Energy Procedia* **2013**, *34*, 740–745.

(84) Shoja Razavi, R.; Loghman-Estarki, M. R. *J. Clust. Sci.* **2012**, *23* (4), 1097–1106.

(85) Ribbing, C. G., Roos, A. *Handbook of opticl constants of solid II*; Orlando Academic, 1991.

(86) R.A. Borzi, S.J. Stewart, R.J. Mercader, G. Punte, F. J. G. *Magn Mater* **2001**, *226*, 1513.

(87) Rakshani, A. E. *Solid State Electron* **1986**, *29*, 7.

(88) B. White, M. Yin, A. Hall, D. Le, S. Stolbov, T. R. *Nano Lett.* **2006**, *6*, 2095.

(89) Heinemann, M.; Eifert, B.; Heiliger, C. *Phys. Rev. B* **2013**, *87* (11), 115111.

(90) Han, K. K., Zhou, Y., Chun, Y., Zhu, J. H. *J. Hazard. Mater.* **2012**, *203*, 341–347.

(91) Dou, B., Song, Y., Liu, Y., Feng, G. *J. Hazard. Mater.* **2010**, *183*, 759–765.

(92) Ghaedi, M.; Ghaedi, a. M.; Hossainpour, M.; Ansari, a.; Habibi, M. H.; Asghari, a. R. *J. Ind. Eng. Chem.* **2013**, *20* (4), 1641–1649.

(93) Kim, D. W.; Rhee, K. Y.; Park, S. J. *J. Alloys Compd.* **2012**, *530*, 6–10.

(94) Ghaedi, M.; Ghaedi, a. M.; Hossainpour, M.; Ansari, a.; Habibi, M. H.; Asghari, a. R. *J. Ind. Eng. Chem.* **2013**, *20*, 1641–1649.

(95) Zahmakiran, M.; Durap, F.; Özkar, S. *Int. J. Hydrogen Energy* **2010**, *35* (1), 187–197.

(96) Zhang, L.; Candelaria, S. L.; Tian, J.; Li, Y.; Huang, Y.; Cao, G. *J. Power Sources* **2013**, *236*, 215–223.

(97) Route, N. R.; Route, N. R. *Adv. Mater.* **2002**, No. 29, 67–69.

(98) Xu, J. F.; Ji, W.; Shen, Z. X.; Tang, S. H.; Ye, X. R.; Jia, D. Z.; Xin, X. Q. *J. Solid State Chem.* **1999**, *147* (2), 516–519.

(99) Zhang, Y. C.; Tang, J. Y.; Wang, G. L.; Zhang, M.; Hu, X. Y. *J. Cryst. Growth* **2006**, *294* (2), 278–282.

(100) Scrocco, M. *Chem. Phys. Lett.* **1979**, *63* (1), 52–56.

(101) Parhizkar, M.; Kumar, N.; Nayak, P. K.; Singh, S.; Talwar, S. S.; Major, S. S.; Srinivasa, R. S. *Colloids Surfaces A Physicochem. Eng. Asp.* **2005**, *257-258*, 445–449.

(102) Yao, W.-T.; Yu, S.-H.; Zhou, Y.; Jiang, J.; Wu, Q.-S.; Zhang, L.; Jiang, J. *J. Phys. Chem. B* **2005**, *109* (29), 14011–14016.

(103) Storck, S.; Bretinger, H.; Maier, W. F. *Appl. Catal. A Gen.* **1998**, *174* (1-2), 137–146.

(104) Stevens, R. W.; Siriwardane, R. V; Logan, J. *Energy and Fuels* **2008**, *22* (12), 3070–3079.

(105) Guo, B., Chang, L., Xie, K. *J. Nat. Gas Chem.* **2006**, *15*, 223–229.

(106) Skoog, D.A., Holler, F.H., Crouch, S. R. *Principle of Instrumental Analysis*, 6th ed.; Kiselica, S., Ed.; David Harris: Canada, 2007.

(107) NIST. COBLENTZ SOCIETY.

(108) Xie, J.; Huang, M.; Kaliaguine, S. **1997**, *115*, 157–165.

APPENDIX A

XPS SPECTRA OF COPPER OXIDES ON SUPPORTS

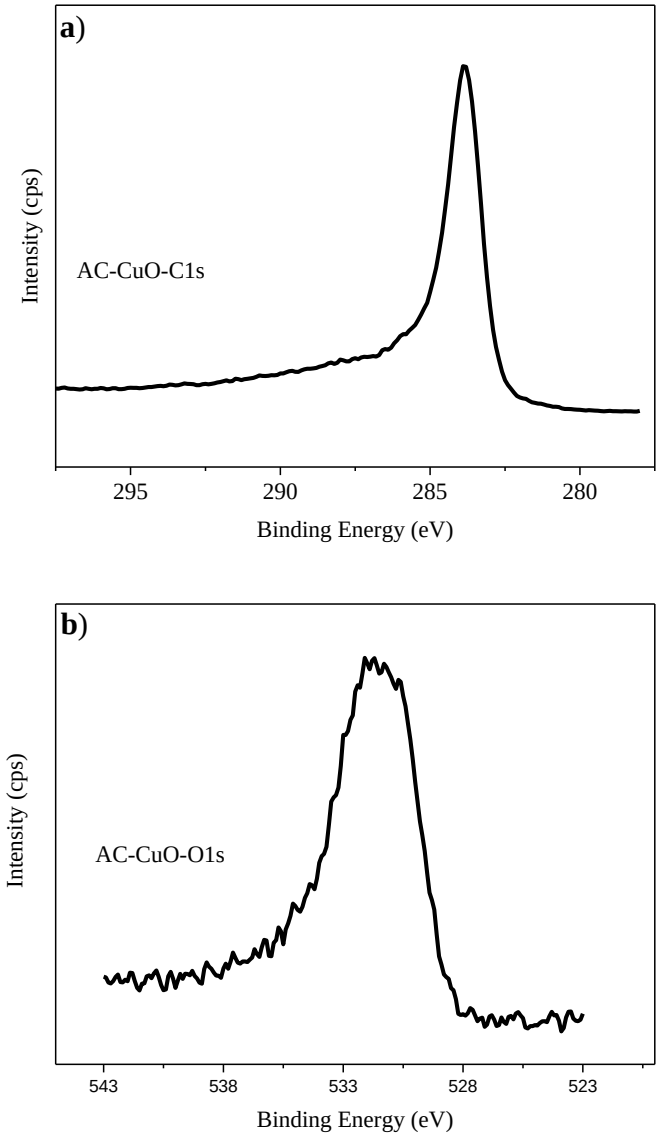

Figure A.1. XPS spectra of activated carbon with CuO, **a)** C1s, **b)** O1s, **c)** Cu2p

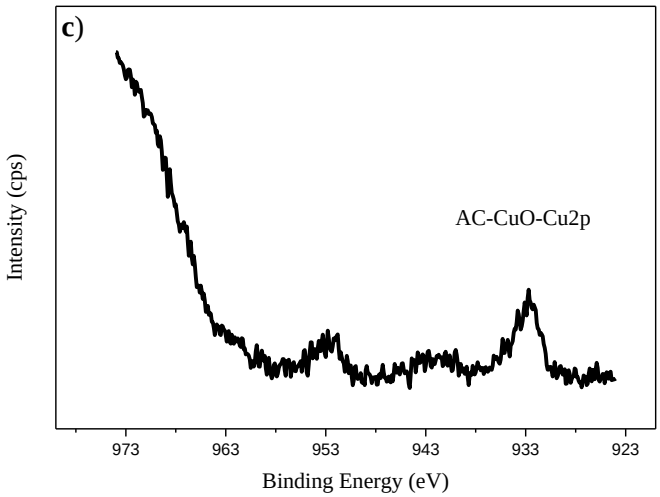

Figure A.1. XPS spectra of activated carbon with CuO, **a)** C1s, **b)** O1s, **c)** Cu2p (continued)

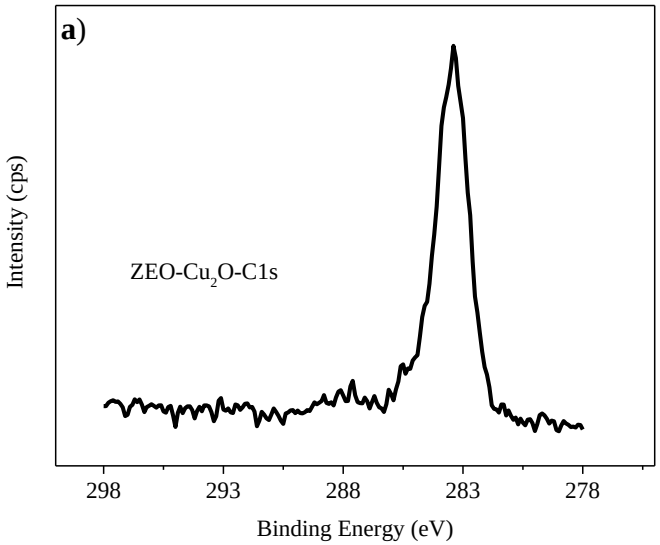

Figure A.2. XPS spectra of zeolite with Cu_2O, **a)** C 1s, **b)** O 1s, **c)** Cu 2p

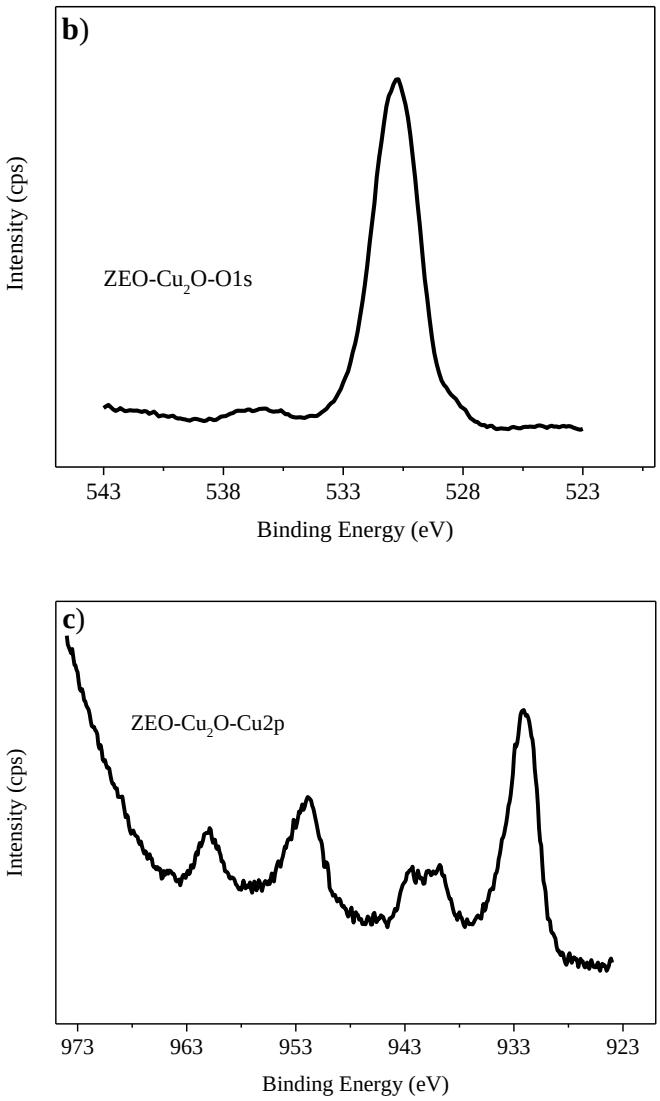

Figure A.2. XPS spectra of zeolite with Cu_2O, **a)** C1s, **b)** O1s, **c)** Cu2p (continued)

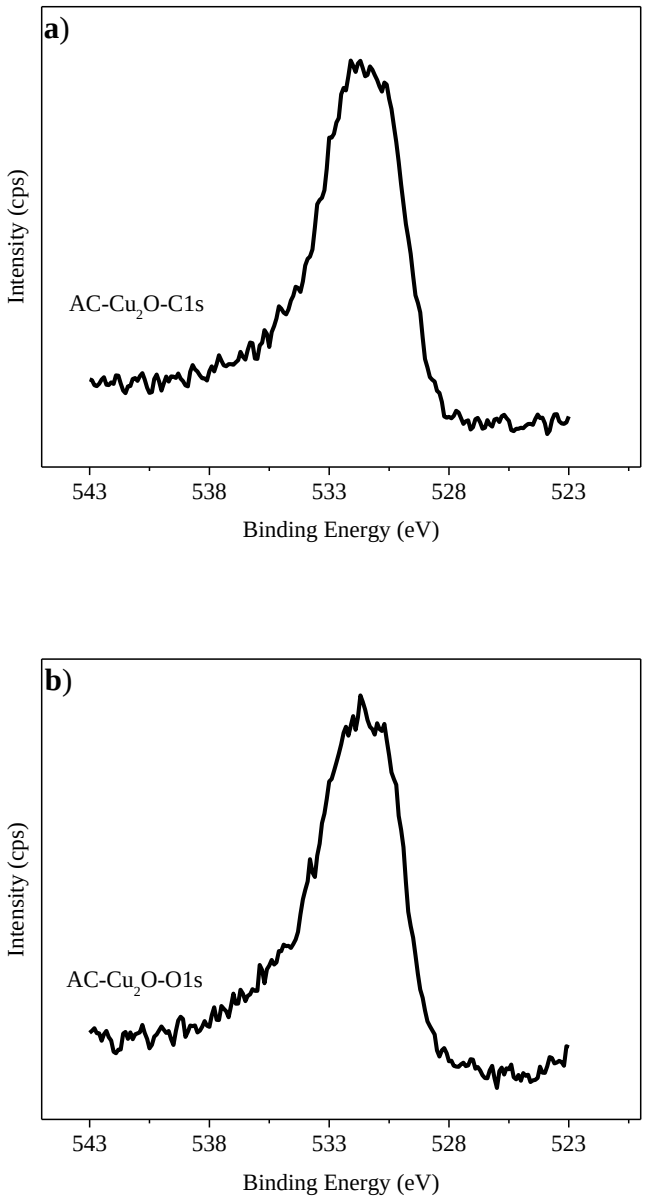

Figure A.3. XPS spectra of activated carbon with Cu_2O, **a)** C1s, **b)** O1s, **c)** Cu2p

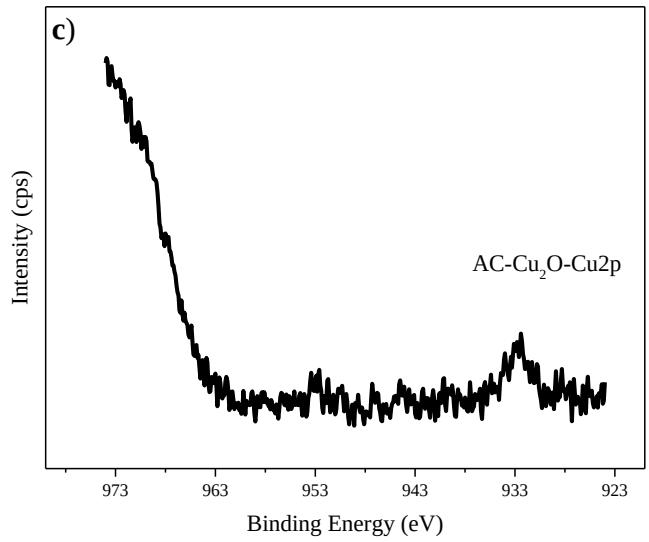

Figure A.3. XPS spectra of activated carbon with Cu_2O, **a)** C1s, **b)** O1s, **c)** Cu2p (continued)

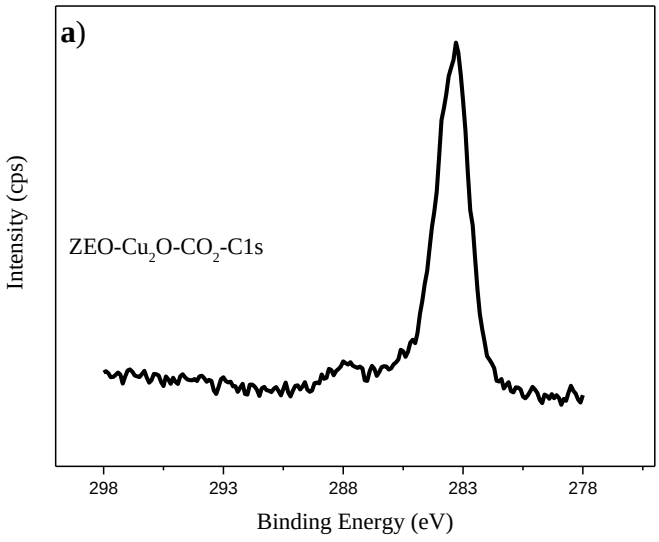

Figure A.4. XPS spectra of zeolite with Cu_2O after adsorption of CO_2, **a)** C1s, **b)** O1s, **c)** Cu2p

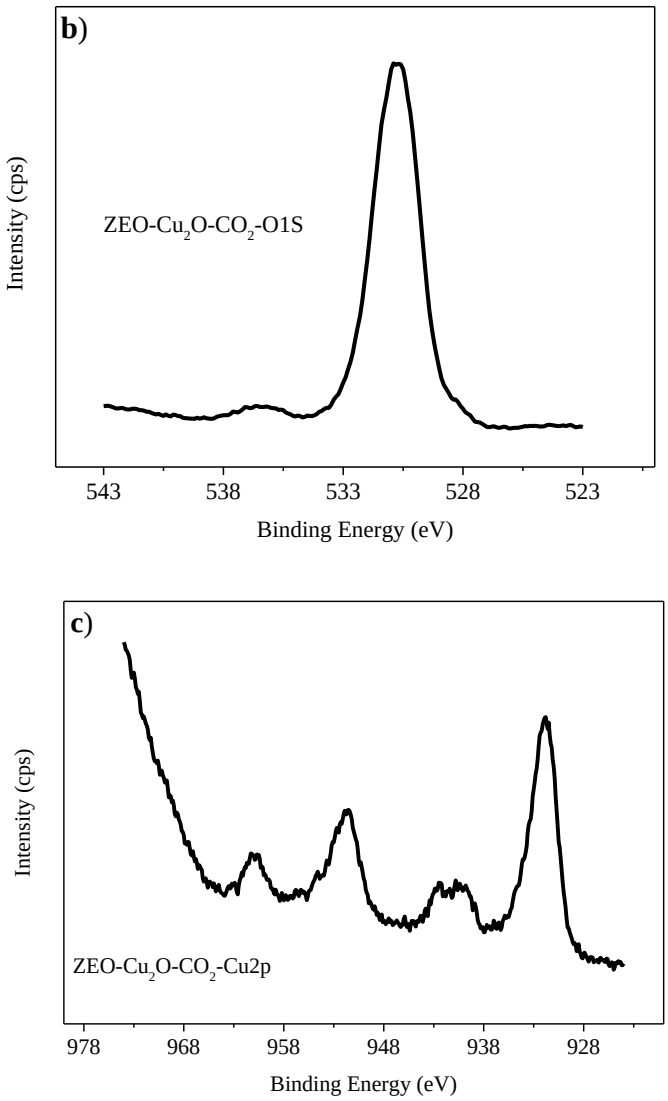

Figure A.4. XPS spectra of zeolite with Cu_2O after adsorption of CO_2, **a)** C1s, **b)** O1s, **c)** Cu2p (continued)